

CHARACTERIZATION OF THE E3 UBIQUITIN LIGASE RNFT2 ORTHOLOG
CG13605 IN *DROSOPHILA MELANOGASTER*

by

Ayşe Kahraman

B.A., Psychology, TOBB Economy and Technology University, 2013

Submitted to the Institute for Graduate Studies in
Science and Engineering in partial fulfillment of
the requirements for the degree of
Master of Science

Graduate Program in Molecular Biology and Genetics

Boğaziçi University

2022

ACKNOWLEDGEMENTS

Firstly, I would like to express my deepest gratitudes to Prof. Arzu Çelik Fuss as she trusted in me from the very beginning of my journey in Bogazici University. Thanks to her, I had the chance to explore many different aspects of science and she was always there whenever I needed her guidance.

I am also thankful to my thesis jury members Assist. Prof. Şükrü Anıl Doğan and Prof. Uygur Tazebay for devoting their time and their valuable feedbacks.

My biggest gratitudes should go to my FlyLab members. I am very thankful to our post-docs Anastasia Fokina and Farzaneh Larti who were always ready to help me with every question in my mind. I also want to thank all of the graduate students, Barış Can Mandacı, Eymen Ece Oruç, Berfin Dağ and Ece Erol who are great people to work with. Even though I met with most of them a short time ago, every minute of being with them was unforgettable.

I cannot thank Barış Can Mandacı, my guardian angel without wings, enough here as pages and words would be insufficient. He can read my mind without any word and made this long journey enjoyable as much as it can be. Whenever I needed a hand in science or in any matter, he was with me. Barış was a great partner both in science and crime. I cannot think of a better friend and feel blessed to know him.

I want to send a tight hug to our great interns, Ayça İrem Küpeli, Gamze Akarsu, Çiğdem Soysal, Gencay Kaan Polat, Yasemin Akın, Didem Özcan, Doğukan Kolçak, Mina Koç and Mert Baysan. Working with each of them was very fun. I especially want to thank Ayça İrem Küpeli as she was like a second pair of hands for me in all of the unending dissections and stainings. Also, I should thank Gamze Akarsu for her unchanging support in and out of lab in every situation.

I want to specifically thank to my previous PI, Prof. Münire Özlem Çevik who was and is a great inspiration for me in many senses. I decided to be a scientist when I first saw her in the first week of my undergraduate studies almost ten years ago. She first made me fall in love with science and then with the flies for both of which I am very grateful. She was also a great mentor in life. I could not be standing where I am right now without her at the beginning.

I also want to send my thanks to Gökhan Özturan who taught me almost everything when I first came to the FlyLab. I thank to my dearest friend Aysu Şevval Alkiraz as she was one of the most sincere joys I was able to meet in Bogazici University. I am also thankful to Elif Darbuka Tula as she helped with the cell culture experiments included in this thesis. I want to send a huge thanks and hug to all MBG department.

Last but not least, I want to thank my family and friends. My dearest sister Reyhan was always supportive with me whenever I felt stressed and lost. She is like a mentor to me in my life for any part of it. My father and my mother also were always reachable in every stressful occasion. I want to send love to my brother Recep Kahraman, his wife Merve Yaprak Kahraman and especially to my newborn niece Zeynep Mercan as she was one of the greatest things that can happen in a person's life. I am grateful to Tuğçe Dinçel, Aslıhan Ataman, Gamze Yaşar, Berkan Çetin, Rabia Taşpınar, Sinem Avcı and Sevde Nur Özbolat for their friendships for life. My cats Tuğçe, Dursun and Duran were my biggest stress relievers during this journey, they are the ones that kept me insane for most of the time.

I want to thank TUBITAK for their financial support on this project (Project no: 119Z309). I was also supported by TUBITAK 2210-A National MSc/MA Scholarsip Program.

ABSTRACT

CHARACTERIZATION OF THE E3 UBIQUITIN LIGASE RNFT2 ORTHOLOG CG13605 IN *DROSOPHILA MELANOGASTER*

Characterized by deficits in both intellectual ability and adaptive behavior, intellectual disabilities (IDs) are one of the major neurodevelopmental disorders with a prevalence of 1-3% worldwide. Development of Next Generation Sequencing techniques provided an important step for the study of ID and identification of ID-related genes. A whole exome sequencing study of 404 consanguineous families with ID led to the identification of a novel ID-related missense variant (cT1150C; p.C384R) in the *RNFT2* gene. *RNFT2* (*RING* finger protein, *transmembrane 2*) encodes a RING finger E3 ubiquitin ligase. Its fly ortholog *Dmel/CG13605* has the same type of RING finger domain (C3HC4) and is predicted to be a ubiquitin E3 ligase. The aim of this study is to characterize the fly orthologue of RNFT2, CG13605, and investigate the role of RNFT2 in ID and the orthology between two proteins. For this aim, first I investigated the expression pattern of CG13605 and observed expression in the mushroom body (MB) Kenyon cells throughout development. Then I conducted loss of function experiments by RNAi knockdown and generating and investigating CRISPR knockout mutants. Knockdown experiments resulted in misguidance defects in the MB lobes. Similarly, knockout experiments also led to various MB phenotypes in α/β lobes. To investigate the orthology between RNFT2 and CG13605, I expressed transgenic wild type and mutant RNFT2 in flies in the CG13605 mutant background. Rescue experiments with wild type RNFT2 resulted in rescue of observed phenotypes, indicating a function-oriented orthology between RNFT2 and CG13605.

ÖZET

E3 UBİKİTİN TANIYICI PROTEİNİ RNFT2 ORTOLOGU CG13605'İN *DROSOPHILA MELANOGASTER*'DA KARAKTERİZASYONU

Hem entelektüel yetenek hem de adaptif davranıştaki eksikliklerle karakterize edilen Zihinsel Engellilik (ZE), dünya çapında %1-3'lük prevalansı ile başta gelen nörogelişimsel bozukluklardan biridir. Yeni Nesil Dizileme tekniklerinin geliştirilmesi, ZE'nin incelenmesi ve ZE ile ilişkili genlerin tanımlanması için önemli bir adım sağlamıştır. ZE'li 404 akraba aile üzerinde yapılan tüm ekzom dizileme çalışması, *RNFT2* geninde ZE ile ilişkili yeni bir yanlış anlamlı varyantın (cT1150C; p.C384R) tanımlanmasını sağlamıştır. *RNFT2* (*RING finger protein, transmembrane 2*), bir RING finger E3 ubiquitin tanıyıcı proteini kodlar. Sinek ortologu *Dmel/CG13605* aynı tip RING finger alanına (C3HC4) sahiptir ve bir ubiquitin E3 tanıyıcı proteini olduğu tahmin edilmektedir. Bu çalışmanın amacı, *RNFT2*'nin sinek ortologu *CG13605*'i karakterize etmek ve *RNFT2*'nin ID'deki rolünü ve iki protein arasındaki ortolojiyi araştırmaktır. Bu amaçla, ilk olarak *CG13605*'in ifade örüntüsünü araştırdım ve gelişim boyunca mantarsı gövde Kenyon hücrelerinde ifadesini gözlemladim. Daha sonra RNA yıkımı ve CRISPR nakavt mutantlarını üretip araştırarak fonksiyon kaybı deneyleri yaptım. *CG13605* susturma deneyleri, mantarsı gövde loblarında yanlış yönlendirme kusurlarıyla sonuçlandı. Benzer şekilde, nakavt deneyleri de α/β loblarında çeşitli fenotiplere yol açtı. *RNFT2* ve *CG13605* arasındaki ortolojiyi araştırmak için *CG13605* mutant arka planındaki sineklerde yabancı tip ve mutant *RNFT2*'yi ifade ettim. Yabancı tip *RNFT2* ile yapılan kurtarma deneyleri, gözlenen fenotiplerin kurtarılmasıyla sonuçlanmış ve *RNFT2* ile *CG13605* arasında işlev odaklı bir ortoloji olduğunu göstermiştir.

TABLE OF CONTENTS

ACKNOWLEDGEMENTS.....	iii
ABSTRACT.....	v
ÖZET	vi
LIST OF FIGURES	ix
LIST OF TABLES.....	xii
LIST OF SYMBOLS	xiii
LIST OF ACRONYMS/ABBREVIATIONS.....	xiv
1. INTRODUCTION.....	1
1.1. Intellectual Disability	1
1.2. Intellectual Disability Modelling with <i>Drosophila melanogaster</i>	3
1.3. Mushroom Bodies of <i>Drosophila melanogaster</i>	5
1.4. RNFT2.....	7
1.5. CG13605	12
2. THE AIM OF THE STUDY	14
3. MATERIALS AND METHODS	15
3.1. Biological Material.....	15
3.2. Chemicals and Equipment.....	17
3.2.1. Chemicals.....	17
3.2.2. Buffers and Solutions.....	17
3.2.3. Oligonucleotide Primers	18
3.2.4. Antibodies and Dyes.....	19
3.2.5. Embedding Media.....	19
3.2.6. Disposable Labware.....	19
3.2.7. Equipment.....	20
3.3. Molecular Biology Techniques	21
3.3.1. DNA Amplification by PCR.....	21
3.3.2. Agarose Gel Preparation.....	22
3.3.3. Agarose Gel Electrophoresis	22
3.3.4. Protein Extraction from Adult Flies.....	22
3.3.5. DNA Extraction from <i>Drosophila</i>	23

3.3.6.	Genomic DNA Extraction (Isopropanol Extraction)	23
3.3.7.	Polyacrylamide Gel Preparation	24
3.3.8.	SDS-Page	25
3.3.9.	Western Blotting	25
3.4.	Histological Techniques	26
3.4.1.	Immunohistochemistry	26
4.	RESULTS	28
4.1.	Analysis of the Expression Pattern of CG13605	28
4.2.	Loss of function Analysis of CG13605 via Downregulation Experiments	34
4.2.1.	Mushroom Body-Specific Knockdown of CG13605	35
4.2.2.	Pan-Neuronal Knockdown of CG13605	37
4.3.	Generation and Characterization of CG13605 Knock-Out Mutants	39
4.3.2.	Molecular Characterization of <i>CG13605</i> Null Mutants	44
4.3.3.	Morphological Analysis of Mushroom Bodies of <i>CG13605</i> Null Mutants	47
4.4.	Generation and Validation of RNFT2 Expressing Flies	53
4.4.1.	Generation of RNFT2 ^{wt} and RNFT2 ^{C384R} Expressing Fly Lines	53
4.4.2.	<i>in vitro</i> Characterization of RNFT2-Expressing Flies	55
4.4.3.	Rescue Experiments with Wild Type RNFT2 Allele	56
5.	DISCUSSION	59
5.1.	Analysis of the Localization Pattern of CG13605	59
5.2.	Functional Characterization of CG13605 with Knockdown Experiments	61
5.3.	Functional Characterization of CG13605 with Knockout Experiment	63
5.4.	Generation and Validation of RNFT2-Expressing Flies and Rescue Experiments	66
	REFERENCES	69

LIST OF FIGURES

Figure 1.1. Color-coded depiction of analog structures in human (left) and fly (right) brains.	6
Figure 1.2. Development of mushroom bodies.....	7
Figure 1.3. Family trees of patients carrying RNFT2 variant.....	8
Figure 1.4. Protein structure of RNFT2.....	9
Figure 1.5. in silico modeling of RING domain of RNFT2.	10
Figure 1.6. Subcellular localization of wild type RNFT2 and its variant in HeLa cells.....	11
Figure 1.7. Comparison of the protein structure of RNFT2 and CG13605 and RING finger domain conservation.	13
Figure 4.1. Schematic representation of CG13605 promoter region and Gal4 vector.....	29
Figure 4.2. CG13605-Gal4 shows reporter gene expression in the larval brain, ventral nerve cord and eye imaginal disc.....	30
Figure 4.3. CG13605 is expressed in Kenyon cells of the mushroom body.....	31
Figure 4.4. CG13605 is expressed in mushroom bodies in the larval and pupal brain.	32
Figure 4.5. CG13605 is expressed in mushroom bodies in the adult brain.	33
Figure 4.6. MB-specific downregulation of CG13605 results in minor abnormalities in the MB lobes.....	36

Figure 4.7. Pan-neuronal downregulation of CG13605 results in β lobe fusion and α lobe thinning and loss.	38
Figure 4.8. Generation of CG13605 null mutants.	40
Figure 4.9. Cross scheme of CG13605 null mutant generation.....	41
Figure 4.10. Gel electrophoresis results of the second screening of the F2 flies.....	43
Figure 4.11. Gel electrophoresis results of the generated mutant lines that were sequenced.	44
Figure 4.12. Genomic representation of deletion and insertions in the mutant lines.	45
Figure 4.13. Polypeptide representations of the generated mutant lines.	46
Figure 4.14. Cross scheme of CG13605 null mutants.	47
Figure 4.15. Observed phenotypes in the mushroom bodies of the mutant lines.	48
Figure 4.16. Results of morphological analysis of mutant lines.....	50
Figure 4.17. Total percentages of observed phenotypes according to each line.	51
Figure 4.18. Examples of the brain phenotype observed in the mutant lines.....	52
Figure 4.19. Representative schemes of Gateway cloning constructs for RNFT2 expressing lines generation.	54
Figure 4.20. Western blot analysis of RNFT2-expressing flies.....	55
Figure 4.21. Cross scheme of genetic rescue experiments.	56

Figure 4.22. Mushroom bodies of rescue flies.....	57
Figure 4.23. Bristle phenotype on the thorax of rescue flies.	58

LIST OF TABLES

Table 3.1. List of fly lines.....	15
Table 3.2. List of chemicals.....	17
Table 3.3. List of buffers and solutions.	17
Table 3.4. List of oligonucleotide primers.....	18
Table 3.5. List of antibodies.	19
Table 3.6. List of disposable equipment.	20
Table 3.7. List of equipment.....	20
Table 4.1. Sample sizes of each group for MB-specific knockdown.....	35
Table 4.2. Sample sizes of each group for pan-neuronal knockdown.	37
Table 4.3. Target loci and sequences of gRNAs.....	39
Table 4.4. Generated mutant lines, number of deleted base pairs, length of frameshift and the presence of an early stop codon.	45
Table 4.5. The numbers and percentages of brain phenotypes observed.	52

LIST OF SYMBOLS

bp	Base Pair
kb	Kilobase
mL	Mililiter
ng	Nanogram
rpm	Revolutions per minute
μg	Microgram
μm	Micrometer
μl	Microliter

LIST OF ACRONYMS/ABBREVIATIONS

ADID	Autosomal Dominant Intellectual Disability
ARID	Autosomal Recessive Intellectual Disability
cDNA	Complementary DNA
DNA	Deoxyribonucleic acid
dNPF	Drosophila Neuropeptide F
GFP	Green Fluorescent Protein
gRNA	Guide RNA
ID	Intellectual Disability
MB	Mushroom Body
PBS	Phosphate Buffered Saline
PCR	Polymerase Chain Reaction
PFA	Paraformaldehyde
RNAi	RNA Interference
RNFT2	RING Finger Protein, Transmembrane 2
shRNA	Short hairpin RNA
UAS	Upstream Activating Sequence
UTR	Untranslated Region
XLID	X-Linked Intellectual Disability

1. INTRODUCTION

1.1. Intellectual Disability

Whenever neurodevelopmental disorders were mentioned, intellectual disorders had been overshadowed by more known disorders such as ADHD (attention deficit/hyperactivity disorder) or autism spectrum disorder until several years ago. For many years, intellectual disability (ID), also known as mental retardation, was not considered as a clinical case but rather as a social issue related to environmental conditions or education (Salvador-Carulla and Bertelli, 2006). When neurodevelopmental disorders were introduced as a broader category in DSM-V, intellectual disabilities were put under this category together with autism spectrum disorder, ADHD, learning disorders and motor disorders (American Psychiatric Association, 2013) and obtained their current diagnostic criteria.

There are three main diagnostic criteria that must be met for intellectual disabilities: deficits in intellectual functioning, deficits in adaptive functioning and onset of these deficits before the age of 18 (American Psychiatric Association, 2013). Intellectual functioning includes reasoning, planning, abstract thinking, problem solving and judgment whereas adaptive functioning mainly comprises of daily life aspects like communication, self-management, social participation and friendship abilities (American Psychiatric Association, 2013). IDs are also accompanied by an IQ score lower than 70, confirmed by clinical assessment and further categorized into mild, moderate, severe and profound ID depending on the severity of the malfunctioning (American Psychiatric Association, 2013). With a prevalence of 1 to 3% in general population (Patel *et al.*, 2020), IDs remain to be a major challenge for societies.

The causes of ID vary from exogenous factors such as malnutrition, maternal alcohol abuse, birth complications or physical traumas during development to genetic causes (Vissers *et al.*, 2015). Up until today, many researchers have been trying to unveil the genetic

causes of ID and various genetic conditions were found to be ID-causing. However, as ID is a spectrum disorder rather than having certain borders in clinical assessment and results from various causes at the same time, genetic diagnosis is still incomplete (Vissers *et al.*, 2015). Genetic diagnosis holds a great importance in the study of ID because it can provide comprehensive knowledge on ID type, prognosis or possible treatment options (Vissers *et al.*, 2015). Technologic advances in the last decade made it possible to identify genetic causes of monogenic forms of ID via genome-wide approaches such as next-generation sequencing (NGS) technologies (Vissers *et al.*, 2015; Jamra, 2018).

The advantages of next-generation sequencing techniques are not limited to this. In societies like Western populations where parental consanguinity is low, the prevalence of ID is also low and the identified causes mainly include copy number variations and *de novo* mutations in single genes (Wieczorek, 2018). In these populations, autosomal dominant ID (ADID) and X-linked ID (XLID) have been paid more attention mostly because autosomal recessive ID (ARID) has a high heterogeneity and low prevalence and also small families making it hard to map any genomic defects (Jamra, 2018; Musante and Ropers, 2013). Next-generation sequencing techniques such as whole exome sequencing are great tools to overcome this challenge. There are more than 2500 identified ID genes up to today and more to be described in the future (Maia *et al.*, 2021).

The proteins encoded by ID-causative genes vary from signaling molecules to chromatin remodeling proteins, from transcription factors to synaptic vesicle components or proteins necessary for synaptic vesicle formation (Raymond and Tarpey, 2006). Some of the earliest identified ID-related genes were signaling molecules like PAK3 and GDI which have a role in the RhoGTPase pathway or proteins like ATRX or RPS6KA3 that are important for chromatin remodeling (Raymond and Tarpey, 2006). More recently, novel transcription factors such as ZNF41 or ZNF674 and various proteins like SLC6A8, NLGN4 or SYN1 which are important for synaptic vesicles and their formation also have been identified as ID-related proteins (Raymond and Tarpey, 2006). Many studies indicate that dysfunctioning in the synapse formation, synapse plasticity and dendrite formation is one of the major contributing factors in ID in which intellectual functioning and behaviors are affected

(Srivastava and Schwartz, 2014). The dynamics of the cytoskeleton, presynaptic vesicle cycling, translational regulation and protein degradation in pre- and post-synaptic neurons and cell adhesion molecules in the synaptic cleft are crucial factors in the functional formation of synapses and further learning and memory mechanisms (Srivastava and Schwartz, 2014). Ubiquitination, as well as deubiquitination, is one of the important mechanisms for normal brain functioning including formation, regulation and maintenance of synapses (Mabb and Ehlers, 2010). The strengthening of the excitatory glutamatergic synapses partly relies on the trafficking of AMPA and NMDA receptors thus on the ubiquitination pathway and various proteins which control this receptor trafficking (Mabb and Ehlers, 2010). Different proteins such as ubiquitin ligase APC/C, E3 ligase RPM-1 and RING ubiquitin E3 ligase Mib2 that take part in ubiquitination processes were shown to be affecting the trafficking of AMPA and NMDA receptors through various pathways including Wnt signaling and MAPK pathway (Mabb and Ehlers, 2010).

1.2. Intellectual Disability Modelling with *Drosophila melanogaster*

Identification of ID-related genes can lead to the characterization of the function of the encoded protein, which is an important step in the establishment of effective therapies to cure the disease. Successful development of genetic or pharmacological therapies partly depends on deciphering the molecular and cellular mechanisms of ID-related genes (Foriel et al., 2015). In vivo and in vitro studies are especially important for characterization of these genes as well as identification of new genes in ID phenotypes (Maia et al., 2021). *Drosophila melanogaster* is one of the most important model organisms in the study of ID and many other diseases.

Regardless of the low levels of anatomical conservation between the central nervous systems of flies and humans, it was found that they share a high level of conservation in ID-related biological mechanisms at the molecular, synaptic and cellular level (Tian et al., 2017). *Drosophila melanogaster* was shown to have homologous genes for 75% of all human disease genes (Tian et al., 2017). Moreover, about 87% of human ID-related genes have orthologues in flies (Bolduc and Tully, 2009). With this genetic resemblance in hand, fruit

flies offer scientists many opportunities in the study of ID. Gene manipulation is rather easy with flies as they have only four chromosomes, a completely sequenced genome and low genetic redundancy compared to vertebrates (Rezával, 2015). This makes it possible to analyze gene function and follow molecular or behavioral phenotypes (van der Voet et al., 2014). Gene manipulation can be controlled temporally and spatially with the help of sophisticated techniques and available libraries and molecular networks of diseases can be dissected via manipulation of two or more different genes at the same time (Restifo, 2005; van der Voet et al., 2014). It is also possible to introduce human variants or whole human genes into the fly genome (Coll-Tané et al., 2019). Flies can generate large numbers of offspring in a really short time and it is cost-efficient to use flies in the laboratory (Rezával, 2015). Thus, one can collect disease-relevant tissues in great quantities for analysis and also conduct experiments at the whole organism level via behavioral assays (van der Voet et al., 2014).

The opportunity of being able to use flies in behavioral experiments holds great importance in ID research. In addition to protocols assessing simple behaviors like larval crawling or negative geotaxis, complex behaviors like learning and memory can be assessed with appropriate protocols (van der Voet et al., 2014). As one of the main hallmarks of ID is learning and memory deficits (Coll-Tane et al., 2019), these protocols become essential to investigate these deficits. Bolduc and Tully (2009) summarized some of the learning and memory assays that are used in ID studies and some of the ID-related genes (like FMR1 in Fragile X syndrome, DYRK1A in Down syndrome and SYN1 in variable learning disabilities), which cause learning/memory deficits in flies (Bolduc and Tully, 2009).

Another opportunity of *Drosophila* in ID researches is that the examination of the neuroanatomy of the diseases can be done thoroughly. One of the fundamental brain structures in mammals involved in learning and memory processes is the hippocampus. Several studies revealed that ID-related genes are important for the proper development and functioning of the hippocampus (Coll-Tané et al., 2019; Bulayeva et al., 2014). In the fly brain, a special structure called mushroom body (MB) is considered to be the major center for olfactory and associative learning, memory formation and consolidation and translation

of sensory input to the learned behavioral responses (Mariano et al., 2020). Even though the general structures of fly and mammalian brains are very different, MBs of the fly brain are often attributed as analogues to the mammalian hippocampus not only because of their similar cognitive roles but also because of their high homologies in gene expression and neural circuitry (Coll-Tané et al., 2019; Figure 1.1). Therefore, MBs became one of the main focuses in ID modeling in *Drosophila melanogaster*.

1.3. Mushroom Bodies of *Drosophila melanogaster*

MBs are bilateral neural structures in the fly brain that consist of approximately 2500 Kenyon cells situated in the posterior-dorsal part of each hemisphere and their axons (Davis, 1993; Keene and Waddell, 2007). Various studies implicate MB function in different processes such as olfactory learning and memory formation as well as visual learning (Heisenberg, 2003) and decision making (Aso et al., 2009). It was also shown that different lobes of the MB store different types of long-term memory that changes according to their temporal properties and molecular effects on the lobes (Akalal et al., 2010). Inputs coming to the MB are altered by reward or punishment via dopaminergic neurons and the output signals are transmitted to the convergent parts of the brain via GABAergic, glutamatergic or cholinergic neurons (Aso et al., 2014) ultimately creating modified behavior (Coll-Tané et al., 2019).

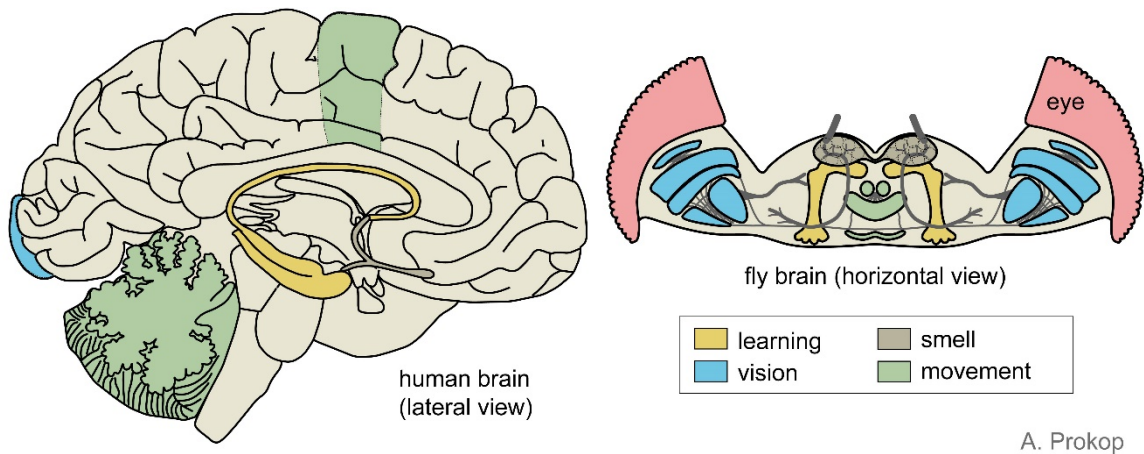


Figure 1.1. Color-coded depiction of analog structures in human (left) and fly (right) brains. Left yellow: hippocampus, right yellow: mushroom bodies (Taken from Manchester Fly Facility resources, 2015).

MBs derive from four neuroblasts in each hemisphere. Each MB neuroblast produces three types of Kenyon cells sequentially: γ neurons are born before mid-third instar larval stage, then α'/β' neurons are born at the late third instar stage and lastly α/β neurons are born at the pupal stage (Lee et al., 1999; Figure 1.2). The axonal projection of each neuron subtype is also sequential. First, γ neurons are born, and their axons are extended towards the anterior of the brain, forming the peduncle. At the heel of the peduncle, they bifurcate: one branch projects medially and the other dorsally. At the early pupal stages these branches of γ neurons are pruned by glial cells and then the axons are projected again but only medially, generating one γ lobe (Hakim et al., 2014). The second group of lobes are formed by α'/β' neurons. They mainly follow the same path of the axons of γ neurons: the axons first project to the peduncle towards the anterior and then bifurcate at the heel of the peduncle medially and dorsally, creating two lobes. The third subtype of neurons, α/β neurons, again project their axons in the same manner: towards anterior through the peduncle and then they bifurcate medially and dorsally. Different from the γ lobes, α/β and α'/β' lobes do not undergo any pruning. At the end, five lobes have formed: dorsally projecting α and α' lobes and medially projecting β , β' and γ lobes (Lee et al., 1999).

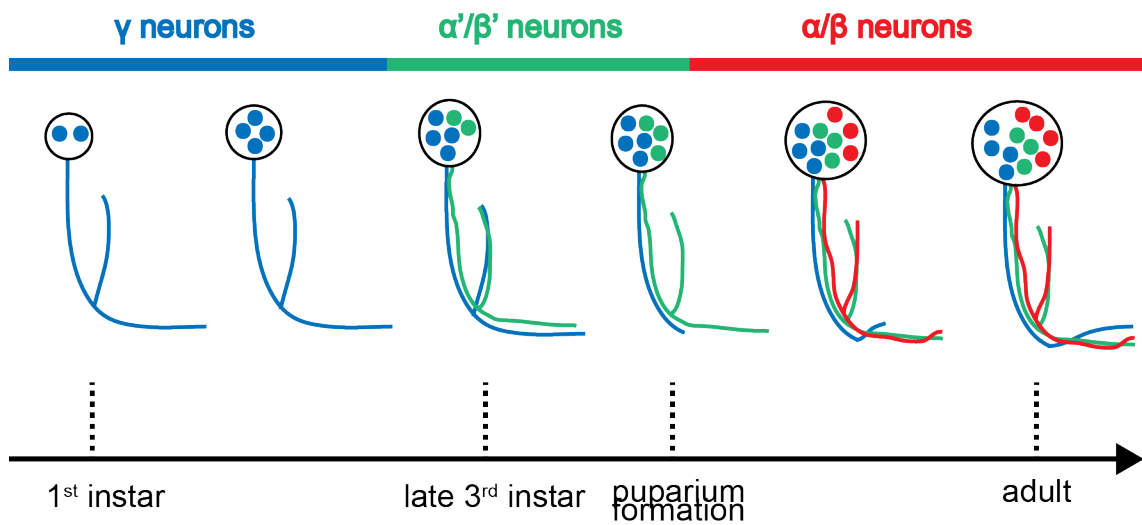


Figure 1.2. Development of mushroom bodies. Three types of Kenyon cells are born and project their axons sequentially. γ neurons (blue) are born first and project their axons. α'/β' neurons are born next at the early pupal stages. Lastly α/β neurons are born after pupae is formed and project their axons (Adapted from Lee et al., 1999).

Any genetic disruption in the Kenyon cells can cause anatomical defects in the MB structure or complete loss of the neurons will affect learning and memory processes in flies (Akalal et al., 2006). Moreover, learning and memory-associated genes are found to be expressed in the Kenyon cells including the famous learning/memory genes *dunce* and *rutabaga* (Davis, 2001; Akalal, 2006). Additionally, when ID-related genes are depleted in flies, their MBs demonstrate different phenotypes such as β lobe fusion and complete or partial loss of α/β lobes (Restifo, 2005, Chubak et al., 2019; Kim et al., 2021) as well as behavioral deficits.

1.4. RNFT2

In 2019, a report on WES and WGS studies conducted with 404 consanguineous families to elucidate genetic causes of ARID was published (Hu *et al.*, 2019). In 219 families, possible disease-causing variants were identified in 77 known and 77 novel candidate ARID genes, 21 X-linked genes and 9 genes previously reported in other diseases (Hu *et al.*, 2019).

RNFT2 is one of the novel candidate ARID genes and has not been linked to any disease yet. Analysis results identified a missense mutation in *RNFT2* (NM_001109903: c.1150T>C) and the same mutation was found in five males from two unrelated consanguineous families in Iran (Hu *et al.*, 2019; Figure 1.3).

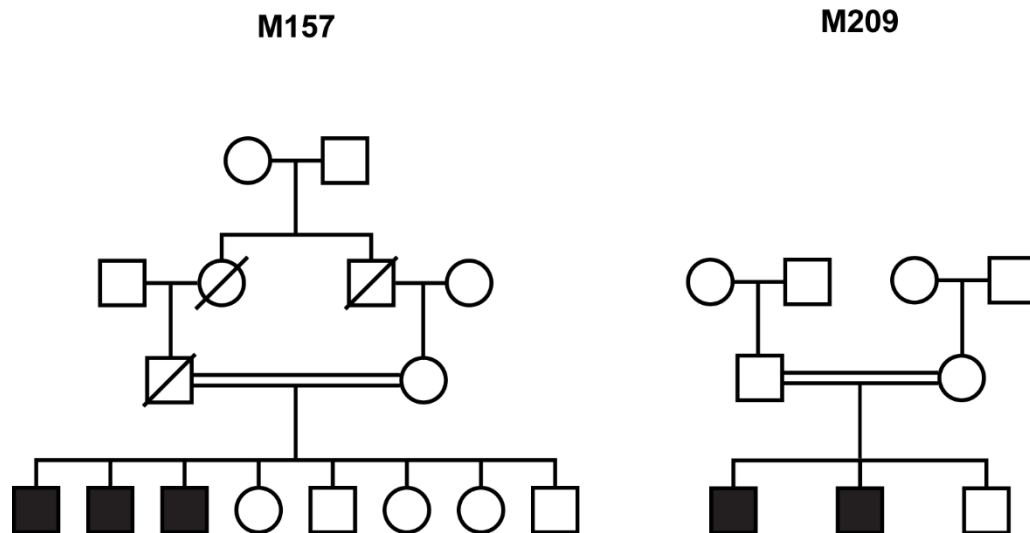


Figure 1.3. Family trees of patients carrying *RNFT2* variant. Five males from two unrelated consanguineous families were found to carry the same missense mutation in *RNFT2* (Adapted from Hu *et al.*, 2019).

Ring Finger Protein, Transmembrane 2 (*RNFT2*, also known as *TMEM118*), encodes a putative E3 ubiquitin ligase. According to the GeneCards database (www.genecards.org), *RNFT2* is predicted to have a role in protein degradation pathway and facilitate ubiquitin protein ligase activity. The expression level of *RNFT2* was found to be significantly higher in brain as compared to other tissues in human (Fagarberg *et al.*, 2014). Several data-sets show the relation between *RNFT2* and neurodegenerative disorders like Alzheimer's disease and schizophrenia (Patrick *et al.*, 2017; Qin *et al.*, 2016). Different studies indicate a possible role in cancer and immune responses (Sasahara *et al.*, 2021; Tong *et al.*, 2020), however no mechanistic studies have been performed to date.

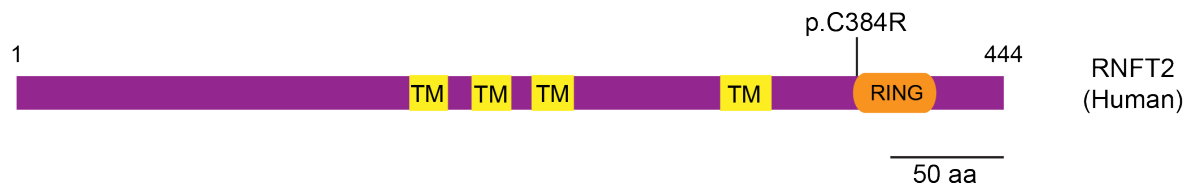


Figure 1.4. Protein structure of RNFT2. In addition to a C3HC4 type RING finger domain, RNFT2 is predicted to have four transmembrane domains. As a result of identified missense mutation, the first cysteine of RING finger domain changes to Arginine.

The RNFT2 protein has four transmembrane domains and a C3HC4 type RING finger domain, which coordinates two zinc ions via conserved cysteine and histidine residues (Figure 1.4). *In silico* analysis of the identified variant in RNFT2 showed that at the protein level, the first cysteine of this conserved RING finger domain was substituted with arginine (NM_001109903: p.C384R). Further analysis via Missense3D algorithm demonstrated that this substitution replaces an uncharged and hydrophobic residue with a charged and hydrophilic residue. As previously reported, the presence of cysteine and histidine residues is important for proper functioning of RING-type proteins (Chasapis and Spyroulias, 2009). Moreover, one of our collaborators showed that both RNFT2 and its identified variant localize to the Golgi apparatus in HeLa cells (Figure 1.6, unpublished data). Thus, the identified mutation in RNFT2 is predicted to affect the binding affinity of RNFT2 to zinc ions and other proteins and therefore its function (Figure 1.5).

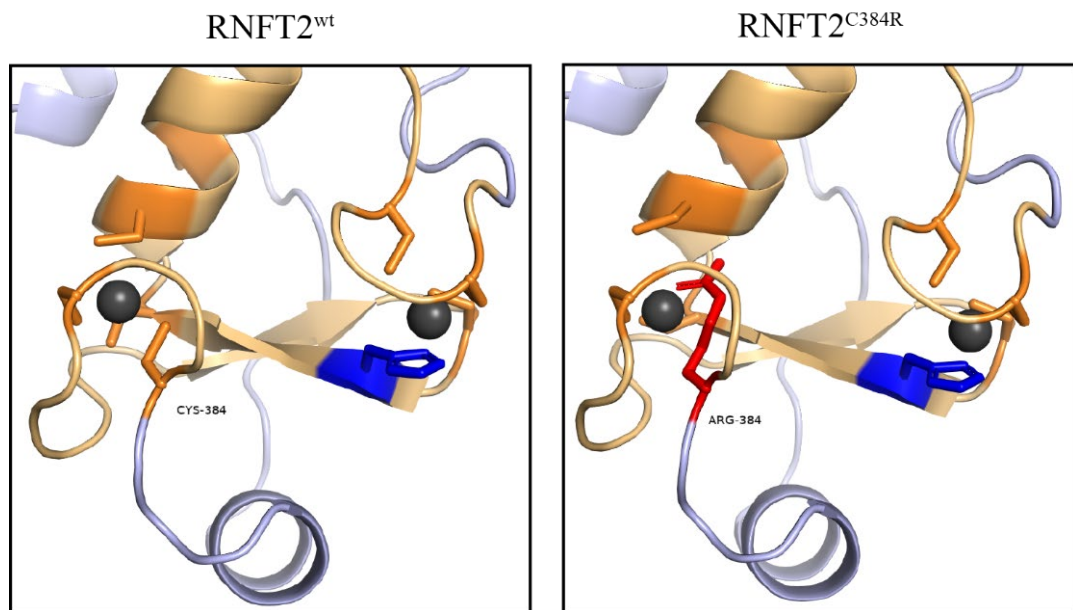


Figure 1.5. *in silico* modeling of RING domain of RNFT2. RING finger domain coordinates two zinc ions (black spheres) via conserved cysteine (orange) and histidine (blue) residues. It is predicted that when the first cysteine of RING domain of RNFT2 changes to arginine, the binding affinity changes.

RING finger domain is a type of zinc finger domain that is known to bind zinc ions via conserved cysteine and histidine residues (Krishna *et al.*, 2003). It was shown that RING finger proteins have divergent roles in ubiquitination, transcriptional regulation, apoptosis, signal transduction and DNA repair via multi-protein assemblies (Matthews and Sunde, 2002). Especially in the nervous system, RING finger proteins have various roles. RING finger protein RNF113a was found to be essential for differentiation and proliferation of neuronal stem cells in mouse brain, its downregulation resulting in cell death (Tsampoula *et al.*, 2022). Downregulation of RNF10 protein, which is also important for synapse morphology and communication between synapse and nucleus, prevents long term potentiation maintenance and structural modifications of dendritic spines (Dinamarca *et al.*, 2016). Several groups showed that RING finger proteins are important factors in neurodevelopment and when disrupted, result in various neurodevelopmental disorders (Jong *et al.*, 1999; Frints *et al.*, 2019; Tenorio-Castaño, 2021). One of the most famous RING-finger proteins is Parkin, whose various mutations result in Parkinson's Disease.

Parkinson's Disease is identified with progressive neurodegeneration and Parkin protein was found to be important for functioning of both pre- and post-synaptic neurons and synapses (Kawabe and Stegmüller, 2021). Also, mutations in the RING domain of Parkin was associated with Juvenile Parkinsonism (Joazerio and Weissman, 2000). Mutations in the RING finger domain of RNF12 was associated with X-linked ID and shown that these mutations are affecting the ubiquitin ligase activity of the protein and further proper functioning (Middleton *et al.*, 2020; Frints *et al.*, 2017; Bustos *et al.*, 2018). As RING finger domain proteins constitute the largest family of E3 ubiquitin ligases and have various roles in most of the cellular mechanisms, mutations in these proteins are widely affecting normal functioning of the cells (Chasapis and Spyroulias, 2009).

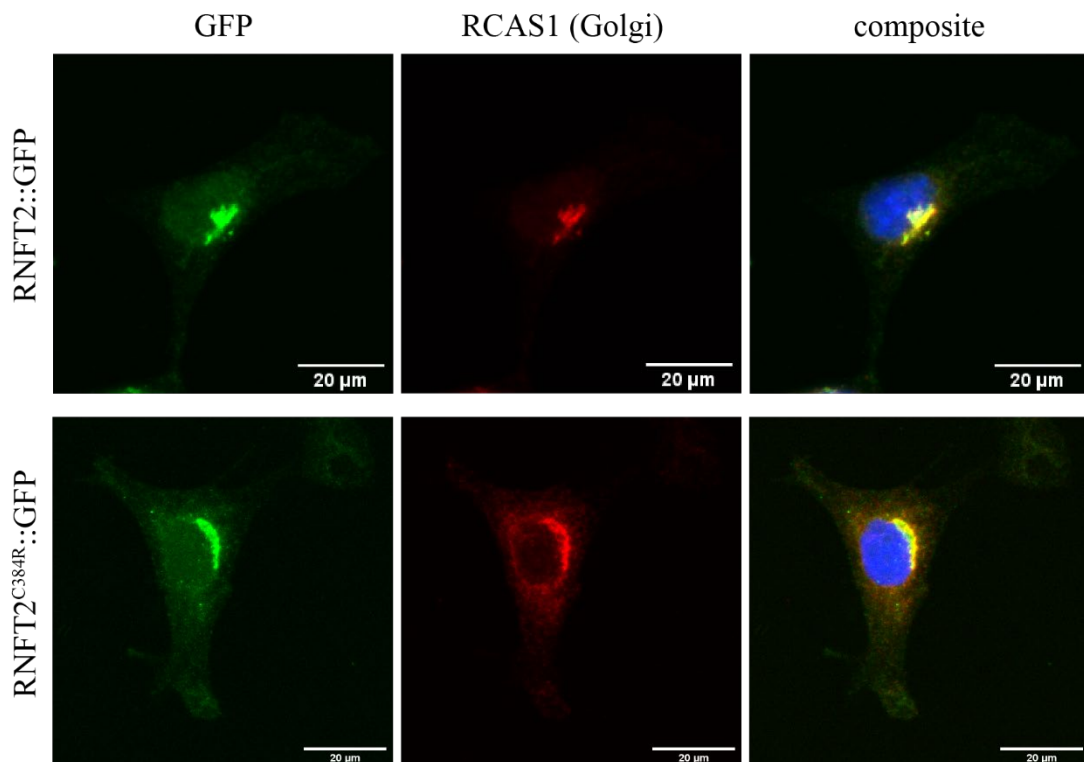


Figure 1.6. Subcellular localization of wild type RNFT2 and its variant in HeLa cells. Both wild type RNFT2 and RNFT2^{C384R} were tagged with GFP. Immunofluorescence results showed that identified mutation does not affect the subcellular localization of RNFT2. Blue represents DAPI staining (unpublished data).

Many RING finger proteins are found to have transmembrane domains, indicating that these proteins are participating in the biological mechanisms of both membrane and membrane-bound organelles like endoplasmic reticulum, lysosome, Golgi apparatus, mitochondria, peroxisomes and endosomes (Nakamura, 2011). Some of the mechanisms transmembrane-RING finger proteins participate in include protein degradation in the endoplasmic reticulum, maintaining of structural integrity of the Golgi apparatus and mitochondria structure, membrane trafficking and apoptosis (Nakamura, 2011). It was shown that one of the RING finger proteins, zinc finger protein-like 1 (ZFPL1), is a structural part of the Golgi apparatus and when downregulated, results in a delay in the ER-to-Golgi trafficking and impairments in the structure of Golgi apparatus (Chiu *et al.*, 2008). Another RING finger protein RNF121 was also found to be localized to the Golgi apparatus and downregulation of RNF121 resulted in an inhibition of cell growth and induction in apoptosis (Zhao *et al.*, 2014). Another study unveiled RNF121 as a new protein involved in the signaling leading to NF- κ B activation, showing overexpression of RNF121 promotes the activity of NF- κ B (Zemirli *et al.*, 2014). These studies also emphasized that RING finger domains were required for the proper functioning of the proteins (Chiu *et al.*, 2008; Zhao *et al.*, 2014; Zemirli *et al.*, 2014). These results indicate that transmembrane-RING finger proteins take part in significant cellular processes especially in the secretory pathway and mutations in their RING domains may be affecting their function.

1.5. CG13605

According to DIOPT Ortholog Finder online tool (flyrnai.org) *CG13605* is the orthologue of *RNFT2* in *Drosophila melanogaster* with a score of 12 out of 15, sharing 39% similarity at protein level (Figure 1.7.A). *CG13605* is located on the third chromosome of the fly genome and its predicted functions are zinc ion binding and enabling ubiquitin ligase activity. It is shown to be expressed in adult fly heads (Aradska *et al.*, 2015). Co-immunoprecipitation analysis indicates *CG13605* is interacting with Wee1, a non-specific protein-tyrosine kinase, which also has a role in protein metabolism and cell proliferation (Sopko *et al.*, 2014). A genome-wide downregulation experiment demonstrated that when

CG13605 is downregulated in S2 cells, more dispersed lipid droplets in smaller size are observed, indicating a potential role for *CG13605* in lipid storage (Guo *et al.*, 2008).

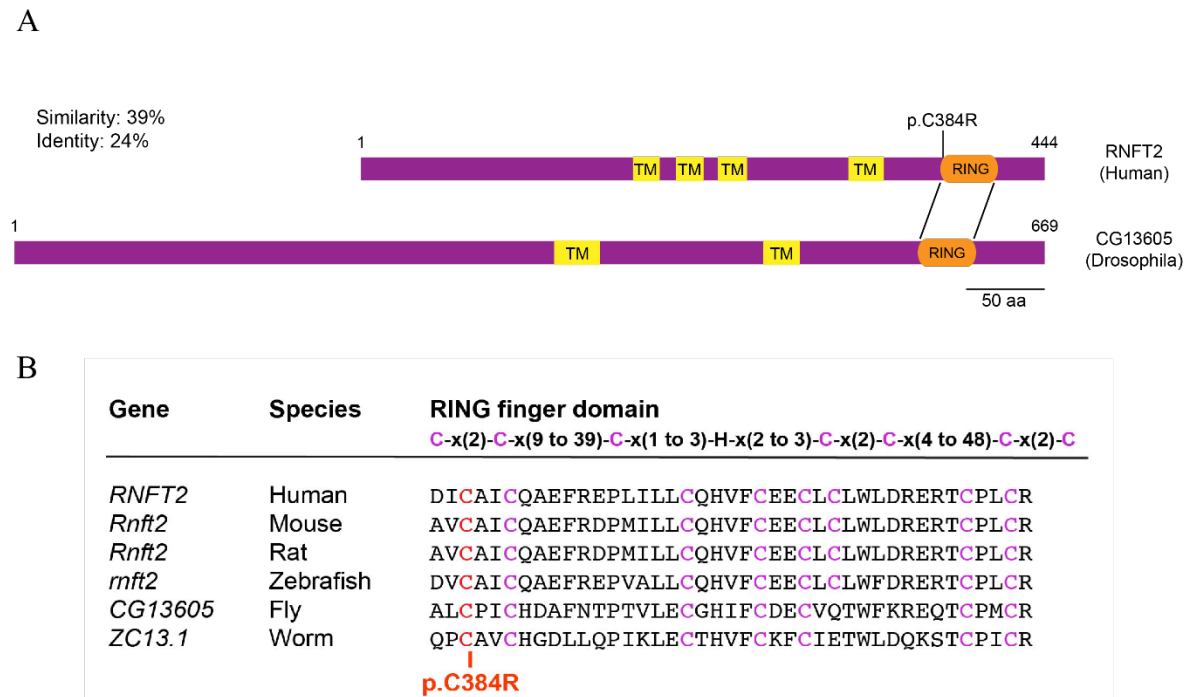


Figure 1.7. Comparison of the protein structure of RNFT2 and CG13605 and RING finger domain conservation. A. RNFT2 and CG13605 were found to have 39% similarity and 24% identity at protein level. In addition to a RING domain, CG13605 is also predicted to have transmembrane domains. B. RING finger domain is conserved between human RNFT2 and its orthologues from other species.

Alignment algorithms showed that RNFT2 RING finger domain is conserved between different species. Its fly orthologue *CG13605* was reported to have a C3HC4-type RING domain (Ying *et al.*, 2011), similar to RNFT2. When the RING finger domains from both of the proteins are aligned and analyzed with online tools, they show a 50% identity with each other (Figure 1.7.B).

2. THE AIM OF THE STUDY

As one of the major neurodevelopmental disorders, intellectual disabilities have been an important research subject for more than 400 years. Elucidation of the genetic causes of ID, especially the autosomal recessive type, has been accelerated with the help of next generation sequencing techniques in the last decade.

In 2019, a variant in the human *RNFT2* gene was reported by the collaborative work of various research groups and classified as a novel ARID-related gene (Hu *et al.*, 2019). The nature of the reported allele and a series of bioinformatic analyses indicated that the variant is likely pathogenic. As no functional study on RNFT2 is conducted yet, understanding its ID-related roles via modeling with flies became my interest.

The aim of this study is to characterize the fly orthologue of RNFT2, CG13605, which is an uncharacterized protein, and thereby gain insight about the possible role of RNFT2 in intellectual disability.

In order to do this, the expression pattern of CG13605 was analyzed via a Gal4 driver line that was generated in our laboratory. Then, knockdown experiments were conducted in a MB-specific or neuron-specific manner. Additionally, CG13605 knockout mutants were generated, characterized and morphologically analyzed to have a better understanding of its function in MB development. Furthermore, human RNFT2 expressing fly lines were generated, validated and then used for rescue experiments in the mutant background. Preliminary results showed that human RNFT2 was able to rescue the *CG13605* mutant phenotype, confirming the orthology between RNFT2 and CG13605.

3. MATERIALS AND METHODS

3.1. Biological Material

Fly lines used in this study, the chromosome numbers of related insertions and descriptions of used lines are listed in Table 3.1.

Table 3.1. List of fly lines.

Name	Chr. No.	Description
Gal4 Drivers		
<i>Elav^{c155}-Gal4</i>	1	Expresses Gal4 protein in post-mitotic neurons under the control of <i>elav</i>
<i>elav.L2-Gal4</i>	3	Expresses Gal4 protein in post-mitotic neurons under the control of <i>elav</i>
<i>CG13605-Gal4</i>	2	Expresses Gal4 protein under the control of the putative promotor sequence of <i>CG13605</i>
<i>c739-Gal4</i>	2	Expresses Gal4 protein in α/β Kenyon cells
<i>c305-Gal4</i>	2	Expresses Gal4 protein in α'/β' Kenyon cells
<i>OK107-Gal4</i>	4	Expresses Gal4 protein in α/β , α'/β' and γ Kenyon cells

Table 3.1. List of fly lines (cont.).

Name	Chr. No.	Description
UAS Lines		
<i>UAS-nLacZ</i>	3	Expresses nuclear localized beta-galactosidase under the control of UAS sequences
<i>UAS-mCD8::GFP</i>	3	Expresses mCD8-tagged GFP under the control of UAS sequences
<i>UAS-RNFT2^{wt}</i>	2	Expresses HA-tagged wild type RNFT2 under the control of UAS sequences
<i>UAS-RNFT2^{C384R}</i>	2	Expresses HA-tagged mutated RNFT2 under the control of UAS sequences
<i>UAS-CG13605^{RNAi}</i>	2	Expresses shRNA for RNAi of CG13605 under the control of UAS sequences
General Stocks and Balancer Lines		
<i>nos-cas9</i>	1	Expresses germ line specific Cas9 protein
<i>w¹¹¹⁸</i>	1	Flies carrying a deletion mutation in their w genes
<i>yw^{QB}</i>		General balancer stock with the genotype of <i>yw</i> ; <i>Sp/CyO</i> ; <i>TM2, Ubx/TM6B, Tb, Hu</i>
<i>BL24640</i>		Conditional virginator and balancer stock with the genotype of <i>w/Y^{hs-hid}</i> ; <i>TM2, Ubx/MKRS</i>

3.2. Chemicals and Equipment

3.2.1. Chemicals

Chemicals used in this study and the manufacturer of each chemical are listed in Table 3.2.

Table 3.2. List of chemicals.

Chemical	Manufacturer
1 kb marker	NEB, USA (N3232L)
100 kb marker	NEB, USA
Agarose	
Bovine Serum Albumin	Sigma-Aldrich, USA (A9647)
EDTA	Sigma-Aldrich, USA (59417C)
Ethidium Bromide	Sigma Life Sciences, USA (E1510)
Isopropanol	
KOAc	
LiCl	
NaCl	Sigma-Aldrich, USA (S7653)
Paraformaldehyde	Sigma-Aldrich, USA (P6148)
Phenol:chloroform:Isoamyl alcohol	Sigma-Aldrich, USA (P2069)
Proteinase K	Roche, Germany (139963000)
Triton-X 100	AppliChem, USA (A4975)
Tween 20	Roche, USA (11332465001)

3.2.2. Buffers and Solutions

Buffers and solutions used in this study are listed in Table 3.3.

Table 3.3. List of buffers and solutions.

Buffer/Solution	Substances
Formaldehyde Solution (4%)	160 g/l PFA, pH 7.4
	1M NaOH until solution becomes transparent

Table 3.3. List of buffers and solutions (cont.).

Buffer/Solution	Substances
PAXD	50 g BSA
	3 g Sodium Dexoycholate
	0.3% Triton X-100 In PBS
PBS (1X)	137 mM NaCl
	2.7 mM KCl
	10 mM Na ₂ HPO ₄
	1.8 mM KH ₂ PO ₄
PBST	PBS (1x)
	0.3% Triton X-100
TAE Buffer (1X)	40 mM Tris-Cl
	1 mM EDTA
	0.1% Acetic acid
Squish Buffer	10 mM Tris, pH 8.0
	1 mM EDTA
	25 mM NaCl
Buffer A	100 mM Tris, pH 7.5
	100 mM EDTA
	100 mM NaCl
	0.5% SDS

3.2.3. Oligonucleotide Primers

Oligonucleotide primers used in this study are listed in Table 3.4. They were synthesized commercially at Macrogen.

Table 3.4. List of oligonucleotide primers.

Name	Sequence
CG13605_A1	AATGAACAACAGCCCAAGG
CG13605_A2	CCGAGCTAGTGTGAAAAGGC
F_CG13605(U6:1)	TATATAGGAAAGATATCCGGGTGAACCTTCGCGGTGTTG GCGCCATACTAGTTTTAGAGCTAGAAATAGCAAG
R_CG13605(U6:3)	ATTTAACTTGCTATTTCTAGCTCTAAACTAGGACTAA ACAGCAATCCGCGACGTTAAATTGAAAATAGGTC
RNFT2-F	CACCATGTGGCTCTTCACAGTGAATCAGGT
RNFT2-R	GTACACCTGGAAGTGTGCGGAC
SDM_rnft2_fw	TGGTGACATCCGCGCCATCTGTCAGGCCGAG
SDM_rnft2_rev	CAGATGGCGCGGATGTCACCAGCTTCTGTGC

3.2.4. Antibodies and Dyes

Antibodies used in this study, their target proteins, hosts, applied dilution and sources are listed in Table 3.5.

Table 3.5. List of antibodies.

Primary Antibodies				
Name	Antigen	Host	Dilution	Source
Anti-Elav	Elav	Rat	1:20	DSHB (7E8A10)
Anti-Repo	Repo	Mouse	1:20	DSHB (8D12)
Anti-GFP	GFP	Rabbit	1:1000	
Anti-FasII	Fasciclin II	Mouse	1:20	DSHB (1D4)
Anti-B-gal	B-galactosidase	Rabbit	1:5000	
Anti-Dach	Dachshund	Mouse	1:10	DSHB (mAbdac1-1)
Anti-HA	HA	Rabbit	1:2000	
Secondary Antibodies				
Alexa 488	Rat	Goat	1:800	Invitrogen
Alexa 488	Rabbit	Goat	1:800	Invitrogen
Alexa 555	Rat	Goat	1:800	Invitrogen
Alexa 647	Mouse	Goat	1:800	Invitrogen
Alexa 647	Rat	Goat	1:800	Invitrogen

3.2.5. Embedding Media

Tissues were mounted in Vectashield Embedding Medium (Vector Laboratories, Inc). Embedded tissues were kept in dark until visualization.

3.2.6. Disposable Labware

Disposable equipment and the manufacturer companies of each are listed in Table 3.6 in alphabetical order.

Table 3.6. List of disposable equipment.

Material	Manufacturer
Micropipette Tips	Greiner Bio-One, Belgium
PCR tubes (200 µl)	Bio-Rad, USA
Pipette Tips (10 - 200 - 1000 µl)	VWR, USA
Plastic Pasteur pipettes	TPP Techno Plastic Products AG, Switzerland
Test Tubes, (0.5 - 1 - 1,5 - 2 ml)	Citotest Labware Manufacturing, China
Test Tubes, (15 - 50) ml	Becton, Dickinson and Company, USA
Filter Tips	Greiner Bio-One, Belgium
PVDF membrane	Roche Life Science
Microscope cover glass	Fisher Scientific, UK
Microscope slides	Fisher Scientific, UK

3.2.7. Equipment

Laboratory equipment and the manufacturer companies of each is listed in Table 3.7 in alphabetical order.

Table 3.7. List of equipment.

Material	Manufacturer
Autoclave	Astell Scientific Ltd., UK
Centrifuges	Eppendorf, Germany (Centrifuge 5424, 5417R)
Confocal Microscope	Leica Microsystems, USA (TCS SP5)
Electrophoresis Equipment	Bio-Rad Labs, USA
Freezers	Arçelik, Turkey
Gel Documentation System	Bio-Rad Labs, USA (Gel Doc XR)
Incubator	Weiss Gallenkamp, USA (Incubator Plus Series)
Laboratory Bottles	Isolab, Germany
Micropipettes	Eppendorf, Germany
Microwave oven	Vestel, Turkey
Refrigerators	Arçelik, Turkey
Stereo Microscope	Olympus, USA (SZ61)
Thermal Cycler	Bio-Rad Labs, USA (C1000 Thermal Cycler)
Cold Room	Birikim Elektrik Soğutma

3.3. Molecular Biology Techniques

3.3.1. DNA Amplification by PCR

Two different DNA polymerases were used in PCR reactions: Q5 High-Fidelity DNA polymerase and OneTaq DNA polymerase. Protocols were based on the manufacturer's guidelines. The melting temperatures (TM) of each primer pair were determined independently based on the kind of polymerase used.

High fidelity PCR reaction were performed using Q5 High-Fidelity DNA Polymerase and were done as follows: 1X Q5 Reaction Buffer, 10 mM dNTPs, 10 mM forward primer, 10 mM reverse primer, 0.02 U/l Q5 High-Fidelity DNA Polymerase, varied quantities of template DNA (depending on the experiment, varying between 0.5 ng and 0.5 μ g), and nuclease-free water (ddH₂O) up to final concentration. PCR reactions were occasionally supplemented with 1X Q5 High GC Enhancer. Standard cycling settings were as follows: an initial denaturation step at 98°C for 30 seconds, a total of 25–35 cycles at 98°C for 10 seconds, annealing temperature dependent on the TMs of primer pairs for 30 seconds and 72°C for 30 seconds each kilobase to be amplified, and lastly a final extension step at 72°C for 2 minutes.

Qualitative PCR reactions were performed with OneTaq DNA polymerase as follows: 1X OneTaq Standard Reaction Buffer, 10 mM dNTPs, 10 mM forward primer, 10 mM reverse primer, 0.025 U/l OneTaq DNA polymerase, varied quantities of template DNA, and ddH₂O. An initial denaturation step at 94°C for 30 seconds, followed by 30 cycles at 94°C for 30 seconds, annealing temperatures based on the TMs of the primer pairs for 1 minute and 68°C for 1 minute per kilobase to be amplified, and a final extension step at 68°C for 5 minutes make up the standard cycling conditions.

3.3.2. Agarose Gel Preparation

Unless otherwise specified, agarose was dissolved in 1X TAE buffer at a final concentration of 1%. The mixture was heated in a microwave, and once it had cooled, ethidium bromide (EtBr) at a concentration of 50ng/mL was added. Then, using a comb, the mixture was put into the proper tray and allowed to set. The comb was taken off once the gel had set, and the gel was then placed into an electrophoresis tank with a tray.

3.3.3. Agarose Gel Electrophoresis

DNA samples were prepared by adding DNA loading dye to a final concentration of 1X. The dye and samples were thoroughly mixed. The samples and a DNA ladder were then loaded to separate wells. According to the predicted band sizes, a 1kb or 100bp DNA ladder was used. 1X TAE buffer was poured into the electrophoresis tank. The samples were run for 50–60 minutes at 90–110V. For the visualization of the gel, a transilluminator was used (Bio-Rad, USA).

3.3.4. Proteion Extraction from Adult Flies

15-20 adult flies were selected carefully and transferred to an Eppendorf tube. The flies were frozen to at -20°C for 5 minutes. 100-140 µl Lysis Buffer was freshly mixed with 1X Protease inhibitor and the mixture was added onto the frozen flies in the Eppendorf tube. By using a pestle, the flies were squashed thoroughly. After they were homogenized, the extract was incubated on ice for 30 minutes. Following ice incubation, the tube was centrifuged at 13000 rpm at 4°C for 10 minutes. After centrifugation, the clear and protein containing part on the bottom was collected with a micropipette while avoiding the lipid-rich upper layer. The collected liquid was transferred into a clean Eppendorf tube. Onto the clear extract, the proper amount of Laemmli's Sample Buffer was added to obtain a final concentration of 1X. Laemmli added extract was then boiled at 98°C for 10 minutes to break

the 2° and 3° structures of the proteins. Also, Laemmli's Sample Buffer contains DTT and β -Mercaptoethanol, which can break the disulfide bonds within or between proteins. Finally, after boiling, the sample was stored at -20°C for further use in SDS-PAGE/Western blotting.

3.3.5. DNA Extraction from *Drosophila*

Single fly: The chosen fly was put in a 200 μ L PCR tube and frozen at -20°C until inactive. For each fly, a solution was freshly prepared by adding 0.5 μ L Proteinase K (20 mg/mL) to 50 μ L Squish Buffer before the extraction. The fresh solution was pipetted with yellow tips, and the fly was mechanically squashed and homogenized with the same tip. The buffer was slowly released into the tube and blended during homogenization. The tubes were then placed in a thermocycler and incubated at 37°C for 30 minutes followed by an inactivation at 95°C for 3 minutes. Using a small centrifuge, the samples were spun for 2 minutes after incubation, and the supernatant was then transferred to a fresh tube. For later use, extracted genomic DNA was kept in a freezer at -20°C.

Wing: Two fly wings were dissected and put into a 200 μ L PCR tube. A solution of 49 μ L of Squish Buffer and 1 μ L of Proteinase K (20 mg/mL) were freshly combined for each tube. To avoid the wings floating on the buffer, the buffer was carefully added into the tube rather than the wings being homogenized. The tubes were incubated in a thermocycler at 37°C for 60 minutes and then at 95°C for 3 minutes. The tubes were kept at -20°C for further use after incubation.

3.3.6. Genomic DNA Extraction (Isopropanol Extraction)

Fifteen carefully chosen flies were put into a 1.5 mL Eppendorf tube and frozen at -20°C. Then, 200 μ L of Buffer A was added to the tubes, and the flies were thoroughly homogenized in this buffer using a homogenizer. After that, the samples were incubated for 30 minutes at 65°C. They were cooled to room temperature after incubation. When the

samples were at room temperature, 114 μL of 5 M KOAc and 286 μL of 6 M LiCl were added, mixed thoroughly, and incubated on ice for at least 10 minutes. The tubes were then centrifuged for 15 minutes at 13000 RPM at room temperature. The supernatant free of fly particles was taken and put into a clean tube. By adding 1 volume of phenol-chloroform (600 μL) to the supernatant, the DNA was extracted. Two phases could be observed clearly when phenol-chloroform was added to the supernatant. The floating phase was then transferred into a clean tube, and the extraction procedure was carried out once more using the same ratio of phenol-chloroform. Isopropanol in a volume of 0.7 was then added, to precipitate the DNA. The tubes were then centrifuged for 15 minutes at 13000 RPM at room temperature. After discarding the supernatant, the pellet was vortexed with 400 μL of 70% EtOH to wash it. The samples were centrifuged once more for 10 minutes at room temperature. The pellet that was left after removing the supernatant was air dried at 37°C until it turned white. The dried pellet was then dissolved in 75 L of ddH₂O and kept at -20°C for further use.

The majority of the genomic DNAs used in this research were isolated from single flies or wings, but on rare occasions when a purer DNA was required, this approach was used.

3.3.7. Polyacrylamide Gel Preparation

To prepare the mold for the gel, two glass plates were held together with a 1 mm of distance between them by a frame and the frame was placed on the standing gasket. First, the resolving gel was poured into the space created between the glass plates and isopropanol was added on top of it to protect the resolving gel from air contact and to smoothen the top edge of the gel before it polymerizes. Once the resolving gel is set, isopropanol was discarded from the top. Onto the set resolving gel, the stacking gel was poured carefully, and an appropriate comb was quickly inserted in the stacking gel between the glass plate before it polymerizes. The fully set gel can be stored at 4°C for further use or it can be directly used in SDS-PAGE/Western blotting.

3.3.8. SDS-Page

For electrophoresis, the polyacrylamide gel is clamped and inserted in the buffer tank. The tank was filled with 1X Running Buffer, which was prepared by diluting 10X Running Buffer with distilled water. The samples were loaded on separate wells along with the prestained protein ladder at the first well to be able to assess the size of the proteins after the electrophoresis. First the gel was run at 80 V and once the samples had passed the stacking gel, the voltage was increased to 120V. The gel was either used in Western blotting or it was stained with Coomassie blue.

3.3.9. Western Blotting

By adding 20% methanol and distilled water, 10X Transfer Buffer was diluted to 1X. To remove SDS from Running Buffer, the acrylamide gel was submerged in water. Methanol was used to activate the polyvinylidene difluoride (PVDF) membrane and after the activation, the membrane was submerged in water to wash the methanol away. Next, the membrane was taken out and incubated in 1X Transfer Buffer. For the transfer of the proteins from the polyacrylamide gel to the PVDF membrane, a gel sandwich was prepared considering the order from the black to the white side of the cassette as follows: 1) Fiber pad, 2) Whatman paper, 3) Protein gel, 4) Methanol activated PVDF membrane, 5) Whatman paper, 6) Fiber pad. The transfer was performed with a current of 200-220 mA for 1.5 hours at 4°C. Ponceau staining, which stains the proteins on the membrane and gives bands that can be observed by naked eye was done to control whether the transfer was successful or not. After the staining, the Ponceau's Red dye was removed and the membrane was washed 3 times, each for 5 minutes with TBS-T. After the washes, the membrane was submerged in 5% non-fat milk powder in TBS-T for 2 hours for blocking. Next, the blocking solution was discarded, and the membrane was washed 3 times, each for 10 minutes with TBS-T. Primary solution was prepared in 5% BSA + TBS-T with the proper dilution ratios suggested by the manufacturer and the membrane was incubated in this solution overnight at 4°C. The next day, primary antibody solution was collected for further experiments and the membrane was washed 3 times, each for 10 minutes with TBS-T. Secondary antibody solution was prepared with

HRP conjugated antibodies and 5% non-fat milk powder + TBS-T solution with the proper dilution ratios according to the manufacturer's suggestion. This solution was added on the membrane, and it was incubated for 2 hours at room temperature. After 2 hours, secondary antibody solution was removed and the membrane was washed in TBS-T 3 times, each for 10 minutes. All washing, blocking and incubation steps were completed on a slow orbital shaker. For the visualization of the membrane, Western Bright ECL was used as HRP substrate and Syngene visualization systems were used at Western blot visualization settings specifically.

3.4. Histological Techniques

3.4.1. Immunohistochemistry

For adult brain staining, 4-10 days old flies were selected carefully and kept on ice to keep them inactive. The dissection step should be maximum 40 minutes for adult brains to make sure that the brains did not get degraded.

For larval brain and imaginal disc staining, third instar larvae were selected carefully and kept on ice in 1X PBS to wash the fly food on them and keep them clean. The dissection step should be maximum 20 minutes for these tissues again for the same reason as adult brains.

Tissues were dissected in cold 1X PBS, and then they were placed in an Eppendorf tube. Next, the dissected tissues were fixed in cold 4% PFA for 30 minutes at room temperature. After fixation, PFA was removed and the tissues were washed for 3 times with 0.03% PBS-T (~300 μ L), which was removed after every 20 minutes followed by the addition of clean PBS-T. After the third wash, PBS-T was removed from the tube and PAXD (~300 μ L) was added for the 30-minute blocking step at room temperature. Primary antibodies were diluted according to the manufacturer's suggestions in blocking solution

(PAXD) and added to the tubes after removing the blocking solution from the tubes at the end the blocking procedure. The tissues were kept in the primary antibody solution overnight at 4°C. The next day, primary antibody solution was removed, and the tissues were washed three times with 0.03% PBS-T, removing it and adding clean solution every 20 minutes. Secondary antibody solution was prepared by diluting the antibodies according to the manufacturer's suggestions (1:800) and added to the tubes after the washing steps. The tissues were incubated in the secondary antibody solution overnight at 4°C in dark. After the secondary antibody incubation, the tissues were washed with 0.3% PBST three times for 20 minutes and two washes for 20 minutes with 1X PBS was done at room temperature, keeping the tubes protected from light. All fixation, washing, blocking and incubation steps were done by putting the tubes on a nutating mixer. For larval tissues, a secondary dissection was performed after these washing steps in 1X PBS. Finally, the tissues were mounted on a microscope slide with Vectashield mounting medium to keep them protected and ready for visualization under confocal microscopy.

4. RESULTS

RNFT2 was initially uncovered by our collaborators in an effort to identify genes underlying intellectual disability. In an attempt to elucidate the function of RNFT2 I chose to study its *Drosophila* homolog CG13605 in the brain.

4.1. Analysis of the Expression Pattern of CG13605

Analysis of the expression pattern of a gene is an important step to understand its function and there are various methods to do this. In flies, one of the most widely used techniques for this aim is the Gal4-UAS binary system, which was also utilized in this study. Mainly, Gal4 is a regulatory protein which specifically binds to UAS and drives the expression of a reporter gene under UAS control. The Gal4 protein can be expressed in a tissue-specific manner when combined with a tissue-specific promoter or enhancer.

For this aim, the region containing the 5'UTR and the sequence between *CG13605* and tRNA:Leu-TAA-2-1 was amplified from fly genomic DNA. Then this fragment was cloned into the P-element vector pBPGUw (Addgene#17575, Pfeiffer *et al.*, 2008) via Gateway cloning (done by Çiğdem Soysal) (Figure 4.1). This vector contains an attB site that can be used for Phi31-mediated site-specific recombination into the fly genome. The vector containing the putative promoter region of *CG13605* and the Gal4 sequence was injected into 250 fly embryos containing an attP landing site on chromosome 2 (landing site VK1(2R)59D3). Injections were performed by the company GenetiVision, USA. Positive transformants were selected according to their eye color and two lines where genomic integration has occurred were provided by the company.

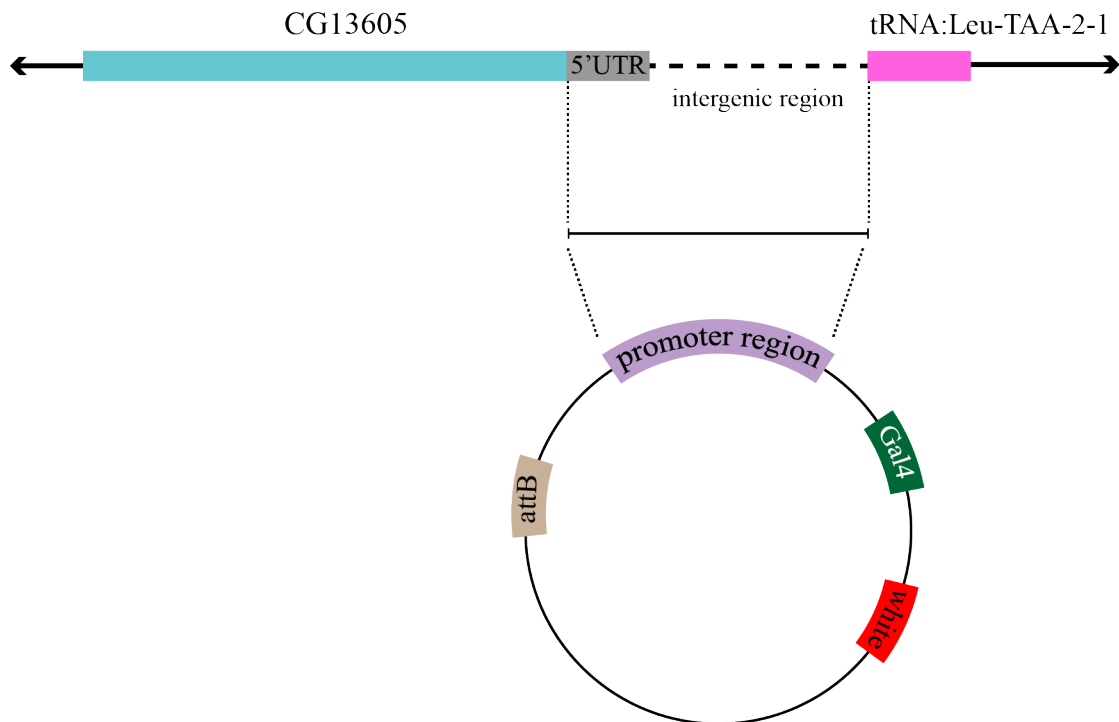


Figure 4.1. Schematic representation of CG13605 promoter region and Gal4 vector. 5'UTR of CG13605 and intergenic region until tRNA:Leu-TAA-2-1 was cloned into the pBPGUw vector which has Gal4 sequences, white gene and attB site.

To identify whether the cloned genomic fragment has promoter activity both transgenic lines were balanced and were later crossed to two different reporter lines. *UAS-mCD8::GFP* (BL32185) expresses membrane-localized GFP, thus making it possible to visualize cell bodies and axons. *UAS-nLacZ* (BL3956) expresses nuclear-localized LacZ, which ensures the visualization of the cell nucleus. Male and female adult flies were analyzed separately to exclude possible gender-specific expression differences.

In order to identify the cells that express CG13605, I stained CG13605-Gal4>UAS-nLacZ third instar larval brains with anti-elav and anti-repo antibodies. I used the nuclear anti-elav antibody to label the nuclei of post-mitotic neurons and anti-repo antibody to detect glial nuclei. I could show that *CG13605* is widely expressed in brain neurons as well as the ventral nerve cord but not in glia (Figure 4.2.A). Even though I did not use Kenyon cell-specific markers in this experiment, I could observe a salient expression coming from the

Kenyon cells (Figure 4.2.A, white rectangles). Furthermore, I observed a high level of expression in the optic lobes, as well as the larval retina (Figure 4.2.B).

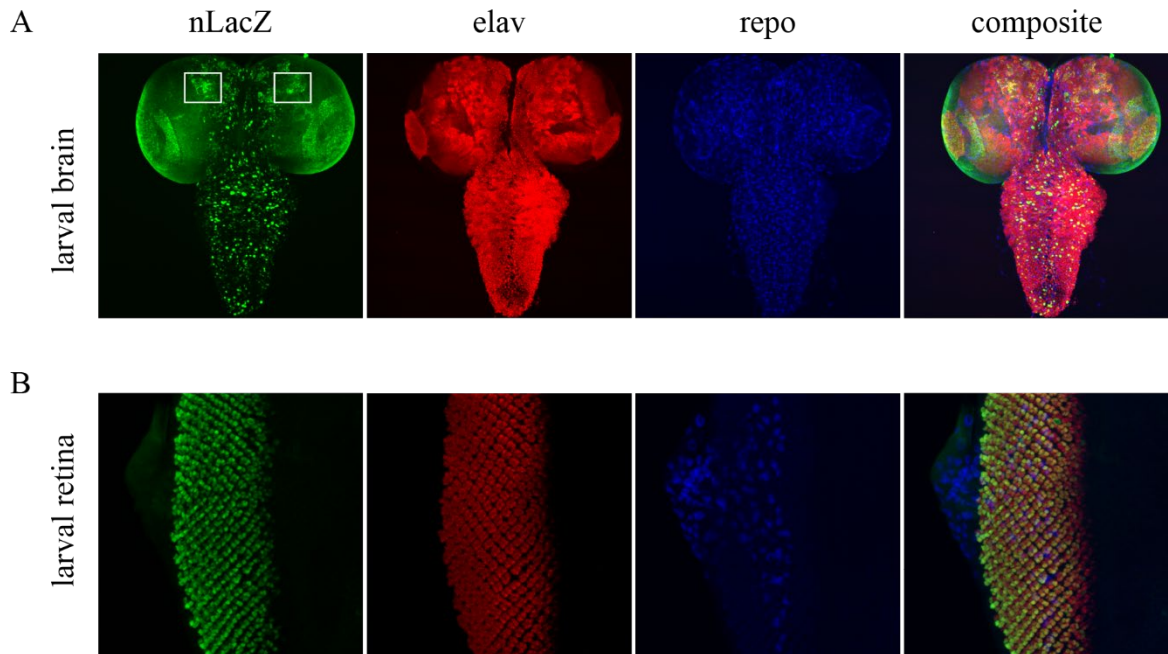


Figure 4.2. CG13605-Gal4 shows reporter gene expression in the larval brain, ventral nerve cord and eye imaginal disc. Triple staining of CG13605-Gal4>UAS-nLacZ flies with anti-b-galactosidase (green) from rabbit, anti-Dachshund (blue) from mouse, and anti-ELAV from rat (red). A. Larval brain and ventral nerve cord immunostainings reveal clear labeling of neurons. White rectangles indicate the area where Kenyon cells are localized. B. Imaginal disc stainings reveal the expression of the nLacZ reporter in photoreceptors.

When I analyzed adult brains of the same genotype, I detected an intense expression in Kenyon cells (Figure 4.3, white rectangle). Co-staining with the anti-dachshund antibody, which mainly stains Kenyon cells as well as other neurons of the circadian clock (Mardon *et al.*, 1994) shows clear co-localization of both markers, however this co-localization was restricted to a subset of Kenyon cells and the expression level of CG13605 varies in different cells (Figure 4.3.B). The question whether this restricted co-localization reflects the endogenous expression of CG13605 or is due to a possible lack of enhancers that could drive expression in all Kenyon cells needs to be further addressed by other experiments. Fifteen

female and thirteen male adult flies were dissected for this experiment and no gender-dependent differences were observed.

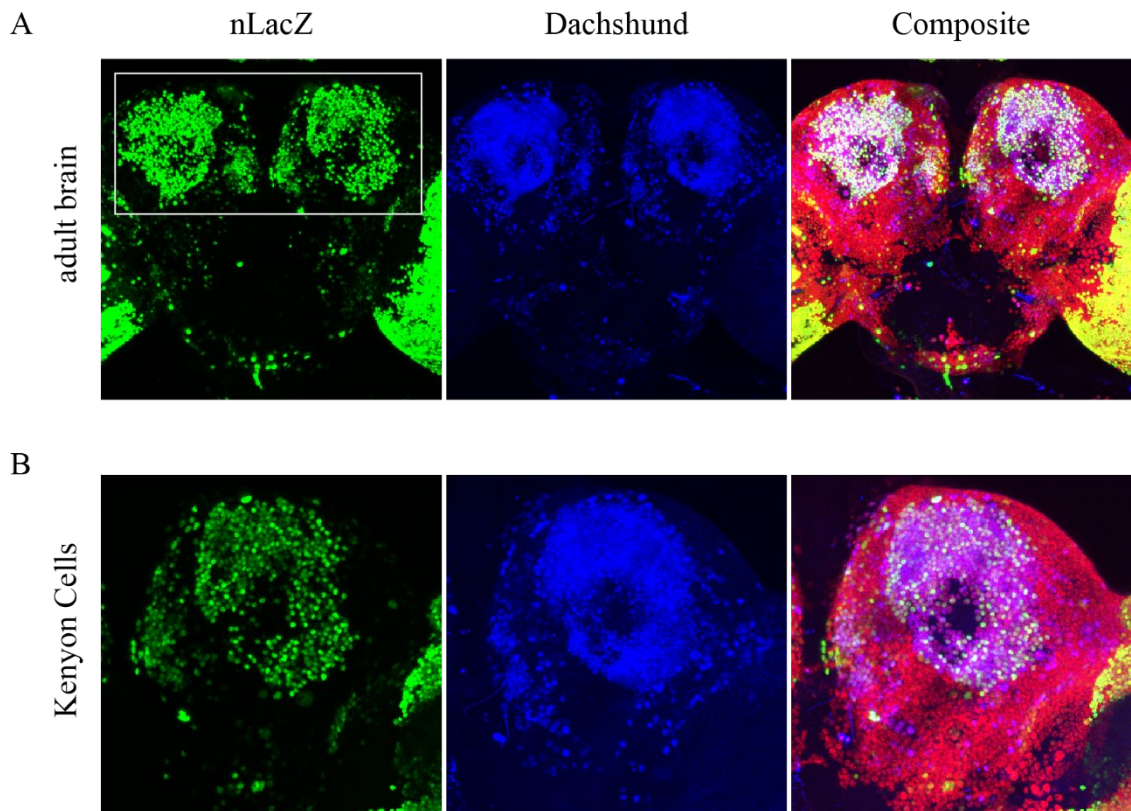


Figure 4.3. CG13605 is expressed in Kenyon cells of the mushroom body. Triple staining of CG13605-Gal4>UAS-nLacZ flies with anti-b-galactosidase (green) from rabbit, anti-Dachshund (blue) from mouse, and anti-ELAV from rat (red). A. Middle part of the adult brain. White rectangle indicates the Kenyon cell area. B. Close-up images of Kenyon cells reveals clearly that only a subset of cells are labelled and expression levels vary between CG13605-expressing cells.

In order to analyze the projections of neurons that express CG13605, I crossed CG13605-Gal4-expressing flies to a fly line that expresses membrane-bound GFP (UAS-mCD8::GFP). I immunostained larval, pupal and adult brains of flies transgenic for both constructs with anti-GFP to visualize axonal projections, anti-Fasciclin II to label the mushroom body, and anti-ELAV to label neuronal nuclei. The anti-FasII antibody labels α/β

lobes intensely and γ lobes faintly. I observed that at all developmental stages, CG13605 is expressed in the mushroom body. In Figure 4, both anti-GFP and anti-FasII antibodies were co-localized in the axons of γ neurons in the larval brain. In the pupal stages the co-localization was found to be further expanding to the α'/β' neurons (Figure 4.4, arrows).

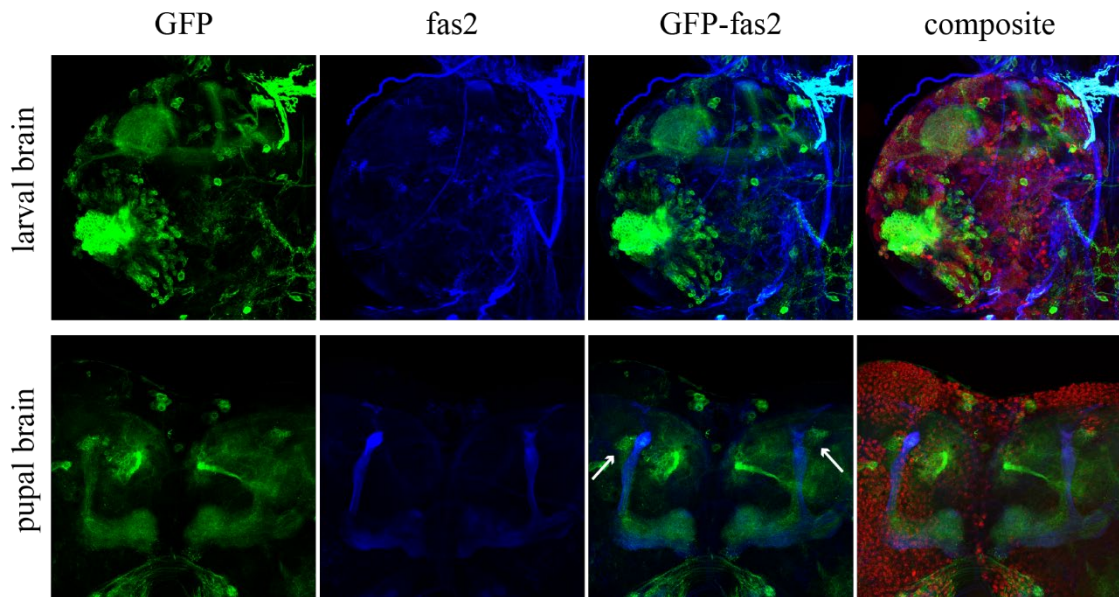


Figure 4.4. CG13605 is expressed in mushroom bodies in the larval and pupal brain. In larval brains, co-localization of GFP and fasII shows that CG13605 is expressed in the γ neurons. Pupal brain stainings show that CG13605 is expressed in α'/β' neurons. Triple staining of CG13605-Gal4>UAS-mCD8::GFP flies with anti-GFP (green) from rabbit, anti-FasII (blue) from mouse, and anti-ELAV from rat (red).

Moreover, the expression of CG13605 was also present in the adult mushroom body (Figure 4.5). The co-localization of GFP and FasII can be seen in all mushroom body lobes. Here, I dissected seven female and seven male adult flies and did not detect any gender-dependent differences.

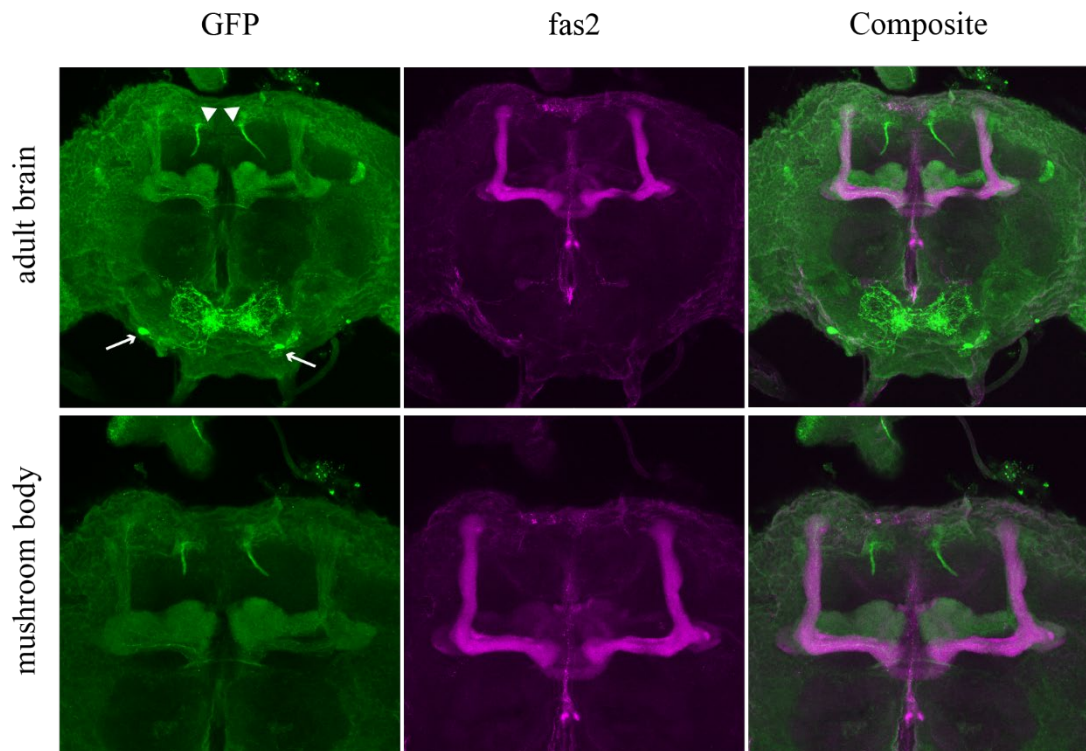


Figure 4.5. CG13605 is expressed in mushroom bodies in the adult brain. The co-localization of GFP and fasII shows that expression of CG13605 is present in the axons of three types of Kenyon cells. Moreover, strong expressions in other cells located in the dorsal (arrowheads) and ventral brain (arrows) can be seen. Double staining of CG13605-Gal4>UAS-mCD8::GFP flies with anti-GFP (green) from rabbit, anti-FasII (magenta) from mouse.

In addition to expression in the MB lobes, highly strong signals were coming from two bilateral cells dorsally located and two bilateral cells ventrally located (Figure 4.5, arrowheads and arrows, respectively). Dorsally located cells, which are also in close proximity to MB α lobe tips, were projecting their axons towards MB Kenyon cells located on the posterior part of the brain. When I checked the literature, I saw that these axons may belong to two bilaterally located *Drosophila* Neuropeptide F expressing cells (dNPF) (Beshel and Zhong, 2013). Neuropeptide F signaling and the dNPFs were shown to have roles in recognition of olfactory and gustatory signals, feeding and sleep-wake behaviors, developmental timing and body size (Chung et al., 2017; Kannangara et al., 2020; Beshel and Zhong, 2013). Different researches also mention the relationship between neuropeptide

F signaling and mushroom bodies and its effects on memory process (Johard et al., 2008; Feng et al., 2021; Krashes et al., 2009). Literature review for the other ventrally located bilateral cells indicated that these two cells may be medial descending neurons which transmit signals from the brain to the spinal cord (Hsu and Bhandawat, 2016). Various studies indicate the role of descending neurons in motor control and sensory-motor coordination (Namiki et al., 2018; Hsu and Bhandawat, 2016). Unfortunately, as we do not have specific markers for both descending neurons and dNPFs in our lab, I could not verify the type of these neurons. Fundamentally, as mushroom bodies are shown to be the main brain structure related to learning, memory and ID diseases, I concentrated on mushroom bodies for further experiments.

In conclusion, localization analysis of CG13605 with Gal4 line showed that it is expressed in the Kenyon cells throughout all developmental stages. When I checked the Kenyon cell expression with nLacZ reporter, I saw that CG13605 is not expressed in all Kenyon cells but in a subset. However, when UAS-mCD8::GFP line was used to detect axonal projections, the expression in the MB looks like it is expressed in all type of Kenyon cells.

4.2. Loss of function Analysis of CG13605 via Downregulation Experiments

In order to understand the function of CG13605, I conducted knock-down experiments. For this, I utilized a transgenic RNA interference line: v105112 (obtained from the Vienna Drosophila Resource Center, KK library) and crossed it with different Gal4 drivers either to downregulate it in all neurons or Kenyon cells. KK library was created with a two-step transformation method: firstly, flies were transformed with a pKC43 vector to generate a target, landing-site carrier line and then shRNA constructs were integrated into the pKC43 target with the help of phiC31-mediated integration (Green et al., 2014). The host line of this library v60100, a carrier for landing site but no shRNA construct, was used as control in our knockdown experiments.

4.2.1. Mushroom Body-Specific Knockdown of CG13605

I utilized MB-specific Gal4 lines to downregulate the expression of CG13605 specifically in Kenyon cells and see any morphological changes. For this aim, I utilized three different Gal4 lines. OK107-Gal4 drives expression in all mushroom body neurons (α/β , α'/β' and γ) and their corresponding lobes (Lee *et al.*, 1999). *c739-Gal4* and *c305-Gal4* lines are subset-specific lines and are used to drive expression in α/β neurons and α'/β' neurons (Aso *et al.*, 2009), respectively. To be able to observe the mushroom body morphology the Gal4-lines were used to drive the *UAS-mCD8::GFP* reporter in addition to the *UAS-CG13605^{RNAi}* construct. Anti-GFP and anti-FasII antibodies were used to detect the morphology of mushroom body α/β and γ lobes. Number of analyzed brains for each group is listed in Table 4.1.

Table 4.1. Sample sizes of each group for MB-specific knockdown.

		<i>OK107-Gal4</i>	<i>c305-Gal4</i>	<i>c739-Gal4</i>
Experimental Group	Female	22	19	22
	Male	23	20	23
Control Group	Female	23	16	19
	Male	21	23	23

MB-specific silencing of *CG13605* by RNA interference resulted in minor abnormalities in mushroom body formation. While downregulation with *OK107-Gal4* and *c305-Gal4* lines showed no observable alteration in the mushroom body lobes (Figure 4.6), downregulation of CG13605 by *c739-Gal4* resulted in thinning of the later-born α/β neurons and α neuron misguidance in the most distal part. I observed that α/β lobe thinning only in female flies with a frequency of 18% (in 4 brains out of 22) (Figure 4.6, arrowhead). On the other hand, α lobe misguidance was observed in both sexes at a frequency of 36% for females, 26% for males (Figure 4.6, arrows). However, I observed the same phenotype in control females with an even higher frequency of 47% (Figure 4.6, arrows), but not in control male flies.

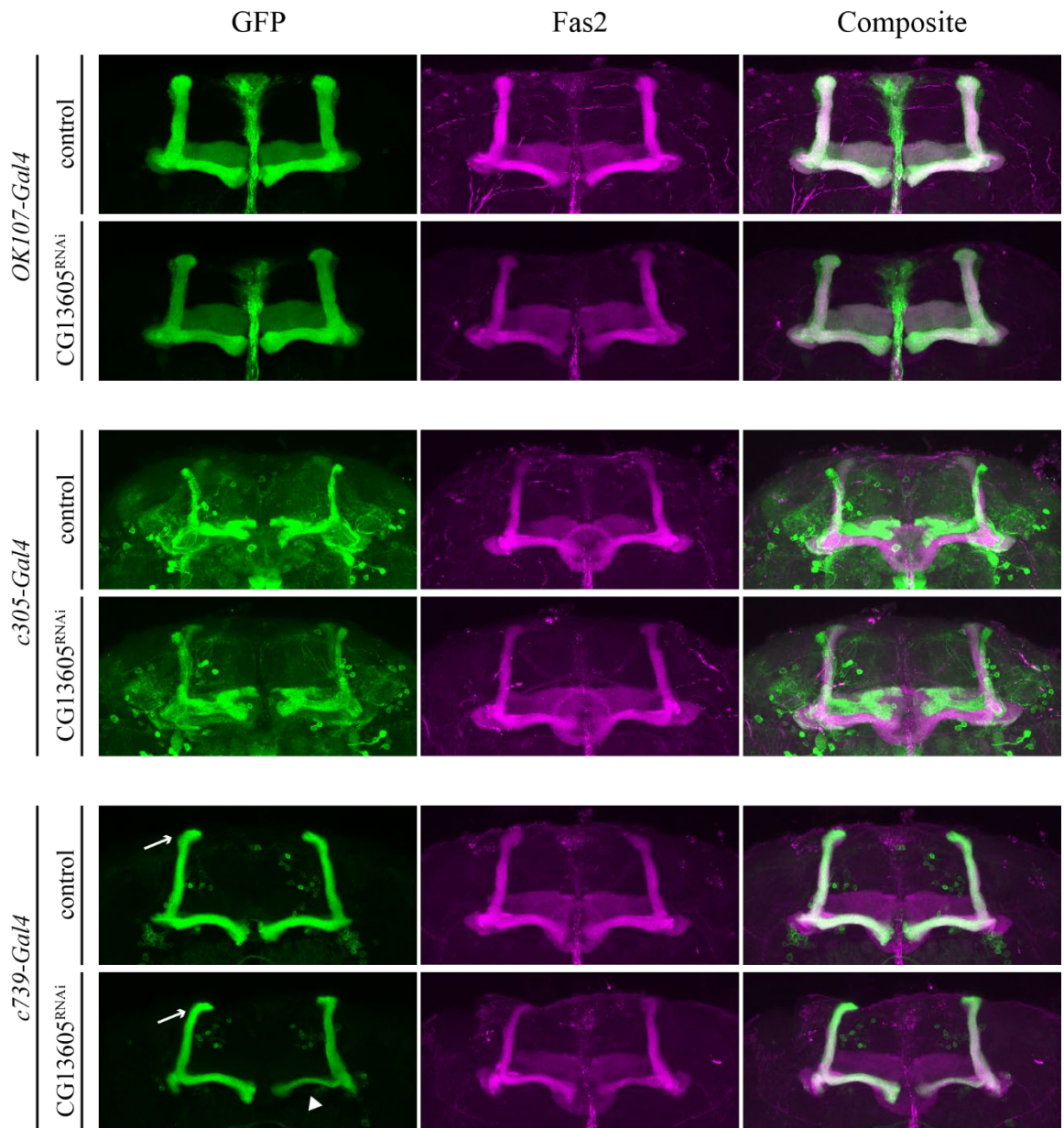


Figure 4.6. MB-specific downregulation of CG13605 results in minor abnormalities in the MB lobes. No observable phenotype was present when CG13605 was downregulated with OK107-Gal4 and c305-Gal4. Only downregulation with c739-Gal4 resulted in minor axon misguidance abnormalities. Double staining with anti-GFP (green) from rabbit, anti-FasII (magenta) from mouse.

4.2.2. Pan-Neuronal Knockdown of CG13605

To investigate the effects of pan-neuronal downregulation of CG13605 on MB development I used the *elav-Gal4* driver, which drives expression in post-mitotic neurons. Elav-Gal4 has been demonstrated to be transiently expressed in embryonic glia (Berger *et al.*, 2007). However, at later stages of development, *elav-Gal4* can be used to drive expression specifically in neurons. I have employed two different *elav-Gal4* lines. The *elav^{CI55}-Gal4* line (BL458) is an enhancer trap insertion in the *elav* gene locus, whereas the *elav.L2-Gal4* is an enhancer fragment that has been cloned to Gal4 (BL8760, Luo *et al.*, 1994). anti-fas2 antibody was used to observe any changes in the α/β and γ lobes of mushroom body. The number of analyzed brains is listed in Table 4.2.

Table 4.2. Sample sizes of each group for pan-neuronal knockdown.

		<i>elav^{CI55}-Gal4</i>	<i>elav.L2-Gal4</i>
Experimental Group	Female	22	13
	Male	18	12
Control Group	Female	17	22
	Male	19	20

When I used the *elav^{CI55}-Gal4* line as a driver, mushroom body phenotypes I only observed phenotypes in male flies. 22% of the brains of male flies showed α lobe loss and β lobe thickening (Figure 4.7, arrowhead). This phenotype is caused by axon misguidance; axons that should extend dorsally and form the α lobe cannot bifurcate at the heel and instead, follow the β lobe neurons. There was no observed phenotype in the mushroom body of the female experimental flies and control flies. When *elav.L2-Gal4* driver line was crossed with RNAi flies, β lobe fusion was observed in 61% of the female flies (Figure 4.7, arrows). Interestingly, in some of the brains with β lobe fusion, we observed thinning in the α lobes (Figure 4.7, star). In males, the same phenotype was observed but the frequency was much lower at around 8%. In controls, no morphological abnormalities were observed in either males or females.

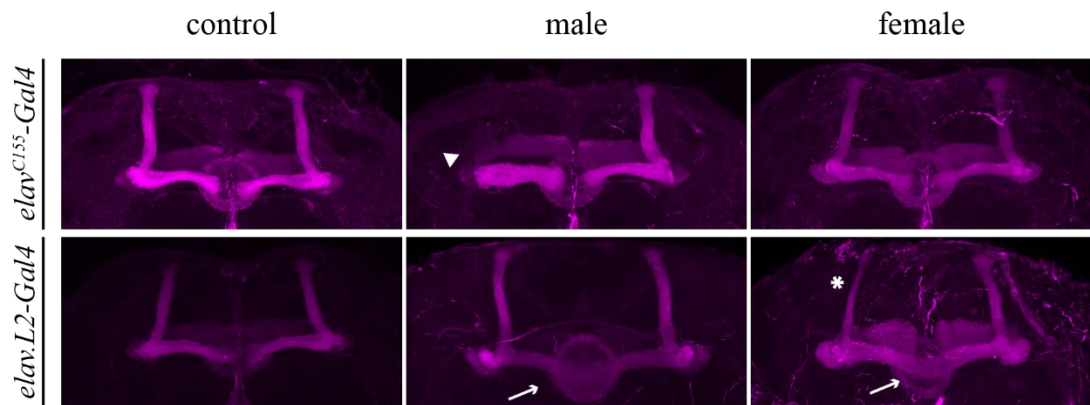


Figure 4.7. Pan-neuronal downregulation of *CG13605* results in β lobe fusion and α lobe thinning and loss. Downregulation with *elav*^{C155}-Gal4 driver resulted in α lobe loss in male flies (arrowhead). *elav*.L2-Gal4 driven downregulation of *CG13605* resulted in β lobe fusion in male and female flies (arrow) and α lobe thinning in female flies (star). Staining with anti-FasII (magenta).

In summary, downregulation of *CG13605* with MB-specific Gal4 drivers did not result in significant changes in the mushroom body morphology. However, pan-neuronal downregulation caused different kinds of misguidance phenotypes of mushroom body neurons with varying penetrance in female and male flies. The differences of the phenotypes may be a result of the downregulation efficiency of the Gal4 lines that have been used and the efficiency of the RNAi line. To increase RNAi efficiency UAS-Dicer could be added to the used genetic background and a second RNAi line could be used. However, as no second RNAi line was available to confirm these results and a knock-out would provide a better of the loss-of-function phenotype I set out to generate and analyze CRISPR knock-out mutants for *CG13605*.

4.3. Generation and Characterization of CG13605 Knock-Out Mutants

4.3.1. Generation of CG13605 Null Mutants via the CRISPR/Cas9 System

In order to disrupt the function of *CG13605* and analyze its effects, I utilized CRISPR/Cas system. I tried to generate null mutants via creating frameshift mutations in the coding region of the gene. For this purpose, the first exon of CG13605 was targeted. The sequence was analyzed by CRISPR Optimal Target Finder tool (targetfinder.flycrispr.neuro.brown.edu). Two guide RNAs (gRNAs) showing highest efficiency and lowest off-targets were selected in order to increase the probability of creating double stranded breaks and frameshift mutations (Figure 4.8, Table 4.3). These selected two gRNAs were separated by 438 bp and predicted to have zero off-targets.

Table 4.3. Target loci and sequences of gRNAs.

Name	Target Locus	Sequence	Off-Target
gRNA1	3R:24111899-24111918 (+)	CCGTAGTATGGGCGCCAACACCG	None
gRNA2	3R:24111441-24111463 (-)	CCATAGGACTAAACAGCAATCCG	None

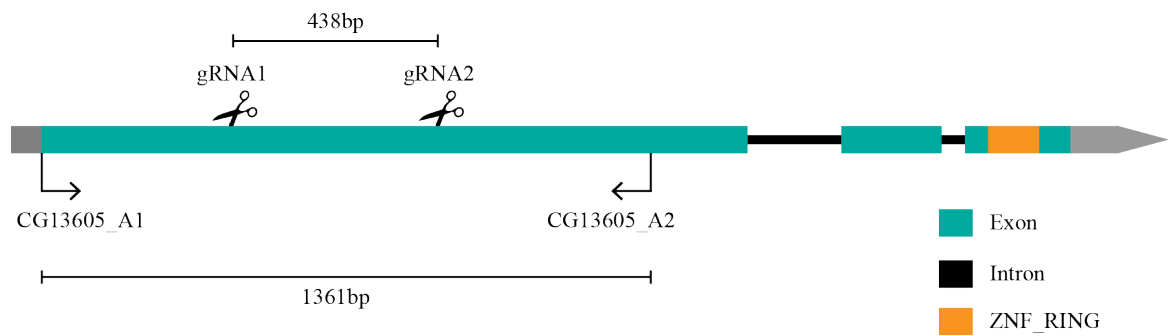


Figure 4.8. Generation of CG13605 null mutants. gRNA target sites and screening primers were shown. gRNAs were separated from each other with 438bp. Depending on the efficiency of gRNAs, various scenarios are expected: if both gRNAs work, a deletion of ~500bp is expected. If only one gRNA works, small indels or point mutations are expected.

After selection, the gRNAs were cloned into the pCFD4 vector which is a tandem expression vector meaning having two gRNA cores and two U6 promoters to enable two gRNA expression at the same time (Addgene#49411, Port *et al.*, 2014; done by Anastasia Fokina). First, a PCR with the primers F_CG13605(U6:1) and R_CG13605(U6:3) using the pCFD4 plasmid as a template was performed. The primers were designed in a way that the forward primer includes gRNA1 and the reverse primer includes gRNA2. They also include 52bps of homology sequences with the plasmid. The amplified fragment was then inserted into a *BbsI* digested pCFD4 plasmid via Gibson Assembly. Cloning of the correct guide RNA sequences was confirmed by Sanger sequencing. Later, the pCFD4 vector carrying two gRNAs was injected into 450 fly embryos. As pCFD4 plasmid has *vermilion* as a selection marker for transgenic lines, injection was performed into flies with a *vermilion* mutant background. With the help of the ϕ C31 integrase system, pCFD4 was integrated into the VK1 docking site on the second chromosome by GenetiVision Corporation (Houston, USA). Two transgenic fly lines carrying the gRNAs were successfully generated.

Male flies from the *CG13605*-gRNA-expressing transgenic line were crossed with *nos-Cas9* female flies (BL54591). *nos-Cas9* flies express Cas9 protein under the control of nanos (*nos*) promoter, which is germline-specific. Double-stranded breaks were expected to

happen in the germ cells of the F1 generation. Male flies from F1 generation which express both Cas9 and gRNAs were then crossed to *ywQB* balancer flies (*yw; Sp/CyO; TM2, Ubx/TM6B, Tb, Hu*) in order to stabilize potential mutations and remove Cas9 and gRNA expressing alleles (Figure 4.9).

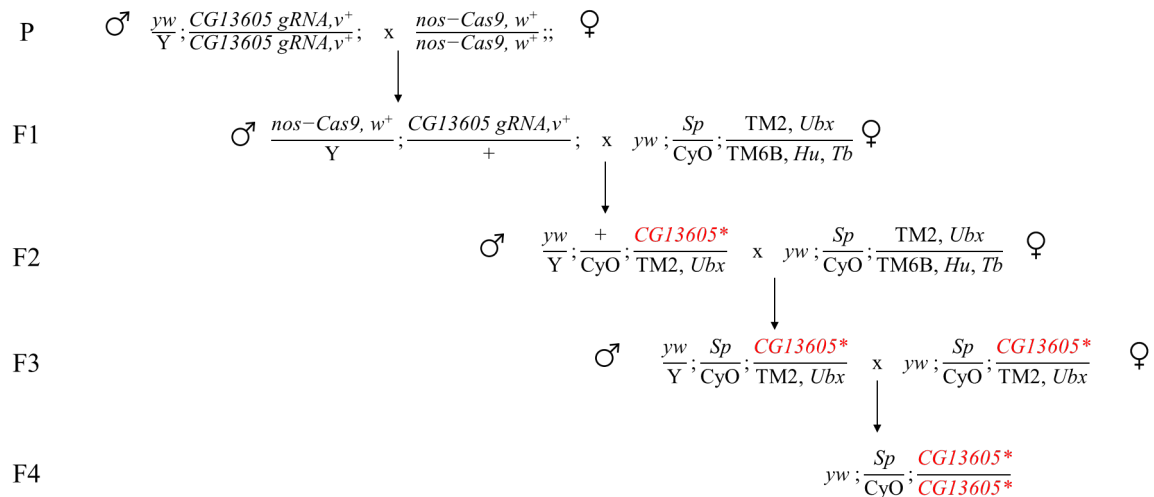


Figure 4.9. Cross scheme of CG13605 null mutant generation. Males carrying gRNAs are crossed with nos-Cas9 carrying females thus double stranded breaks would occur in the germ-line of F1 flies. Then possible mutation carrying flies are crossed with *ywQB* balancer flies.

As every single fly descending from this cross carries a mutation in CG13605 potentially, each of them should be screened. For the mutation screening, a pair of primers flanking the gRNA target sites were designed (Figure 4.8). Several outcomes are possible. As two guide RNAs were used, depending on their efficiency either only one of them or both of them could work at the same time. If both guide RNAs work efficiently a deletion would be expected that would easily be observable on an agarose gel after PCR amplification. While if only one of them worked only smaller indels would result that are usually not detectable on an agarose gel. As flies in the F2 generation were screened one would expect the flies to be heterozygous and to observe both alleles on the gel. Different changes could possible happen to individual alleles and result in trans-heterozygous mutants.

I screened F2 flies after genomic DNA extraction and using primers CG13605_A1 and CG13605_A2 in a single fly PCR. PCR products is run, it is possible to see two bands on the agarose gel because of this heterozygosity: a band corresponding to the wild-type allele with a length of 1361 bp and a second band corresponding to the mutant allele with a length of ~0.9 kb in the case of both gRNAs working. If only one gRNA works, we expect to observe small indel mutations or point mutations in the genomic region.

As a first step, genomic DNA from the wings of 76 male flies of F2 generation was extracted and used as a template in the first screening PCR along with the primers CG13605_A1 and CG13605_A2. 32 of them were found to be susceptible for carrying indel mutations and crossed with *ywQB* females individually in order to increase the number of progeny. A second PCR screen with wing DNAs of three F3 males from each cross with the same primers was performed (Figure 4.10).

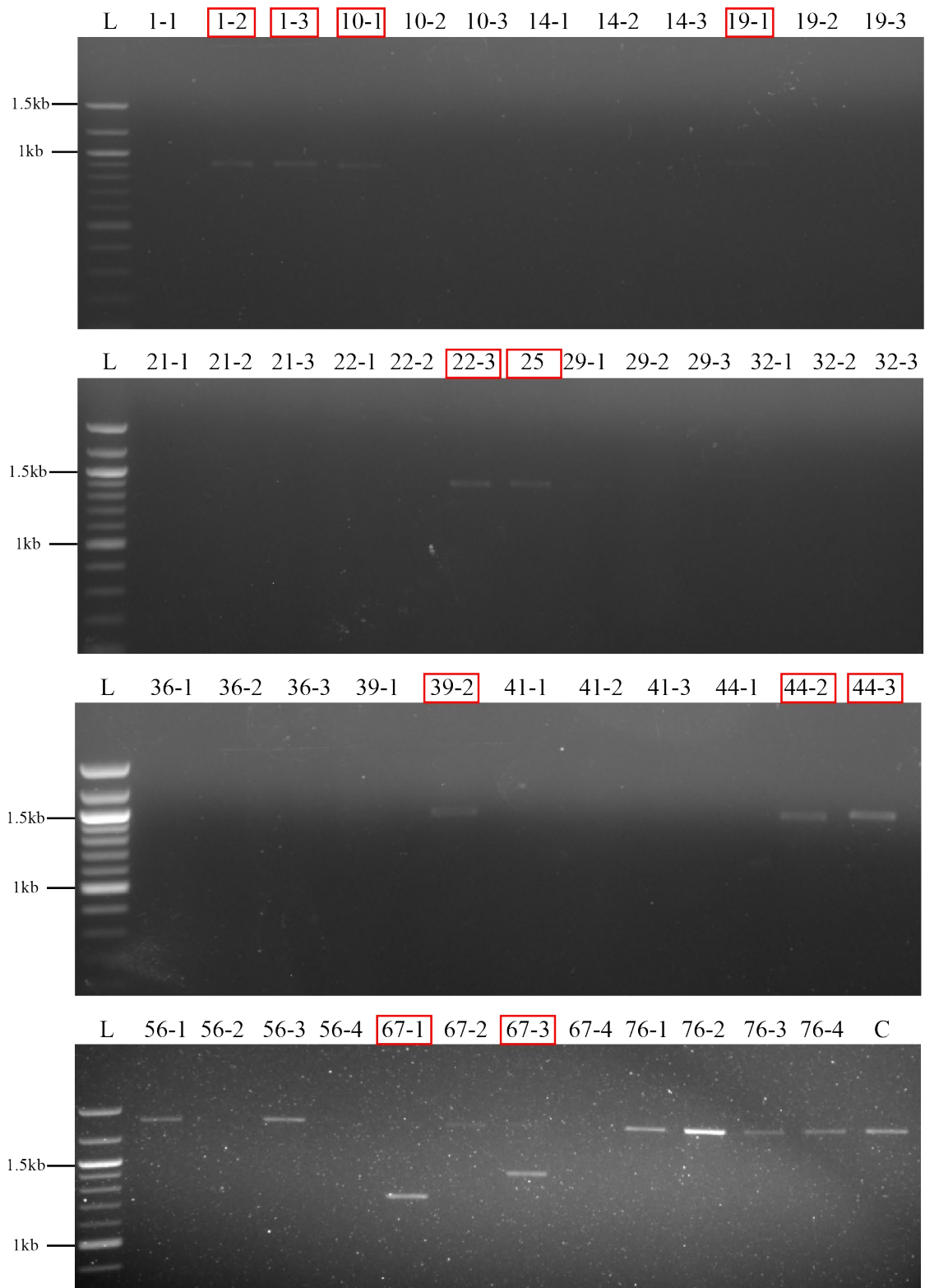


Figure 4.10. Gel electrophoresis results of the second screening of the F2 flies. Red rectangles indicate candidate mutant lines, all showed a deletion of ~500bp. Expected band size for wild type allele is 1361bp. L: 100bp ladder. C: Control with Canton-S DNA.

Out of 32 lines, 11 showed possible deletions in *CG13605* and were individually crossed with *ywQB* balancer flies. Three of these individual crosses were lost because of contamination. Single fly genomic DNA extraction was performed with the progeny of the remaining eight mutant lines to increase the quality of PCR results for sequencing (Figure 4.11).

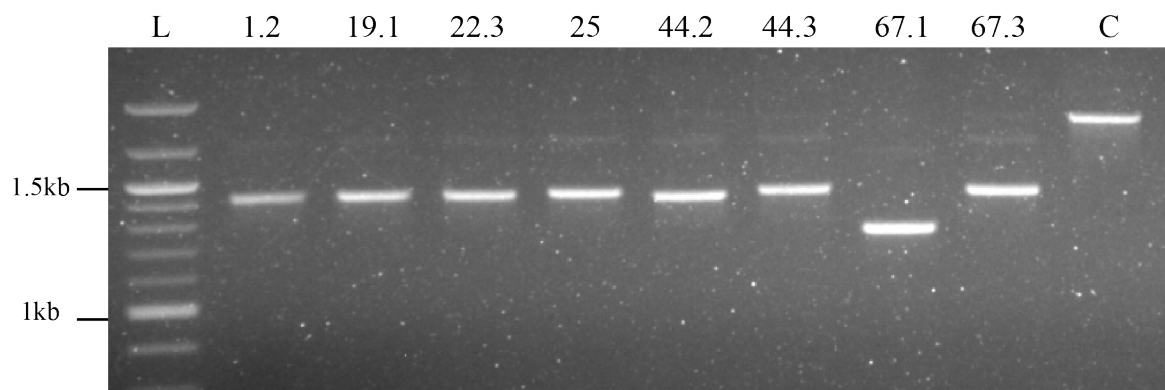


Figure 4.11. Gel electrophoresis results of the generated mutant lines that were sequenced. All eight lines showed a deletion of ~500bp. L: 100bp ladder. C: control with Canton-S DNA.

Purification and sequencing of PCR products were done by Macrogen Inc. (Seoul, Korea). Sequencing results were analyzed using SnapGene software (from Insightful Science; available at snapgene.com). The online tool ExPASy was used for *in silico* translation of the analyzed sequences.

4.3.2. Molecular Characterization of *CG13605* Null Mutants

Analysis of sequencing results revealed that a varying number of nucleotide deletions between the gRNAs target sequences has occurred and resulted in frameshift mutations (Table 4.3, Figure 4.12). All of the lines display deletions of sequences between the two gRNAs showing that both of the gRNAs worked efficiently. In addition to the deletion between gRNAs, the line *CG13605^{m67.1}* also showed a deletion of 167 bp downstream of the

gRNA2. Some of the lines also showed insertion mutations of varying numbers of base-pairs: 5 bp in *CG13605^{m25}*, 11 bp in *CG13605^{m44.3}*, 5 bp in *CG13605^{m67.1}*, and 1 bp in *CG13605^{m67.3}*. All of the insertions were observed around the gRNA1 target region. Different from the other lines, *CG13605^{m1.2}* only showed a 460 bp deletion between gRNAs which results in an early stop codon without any frameshift mutation.

Table 4.4. Generated mutant lines, number of deleted base pairs, length of frameshift and the presence of an early stop codon.

Line	No. of deleted base pairs	Length of frameshift	Early stop codon?
<i>CG13605^{m1.2}</i>	460	0	Yes
<i>CG13605^{m19.1}</i>	464	13	Yes
<i>CG13605^{m22.3}</i>	468	0	No
<i>CG13605^{m25}</i>	466	14	Yes
<i>CG13605^{m44.2}</i>	479	9	Yes
<i>CG13605^{m44.3}</i>	468	1	Yes
<i>CG13605^{m67.1}</i>	645	32	Yes
<i>CG13605^{m67.3}</i>	464	91	Yes

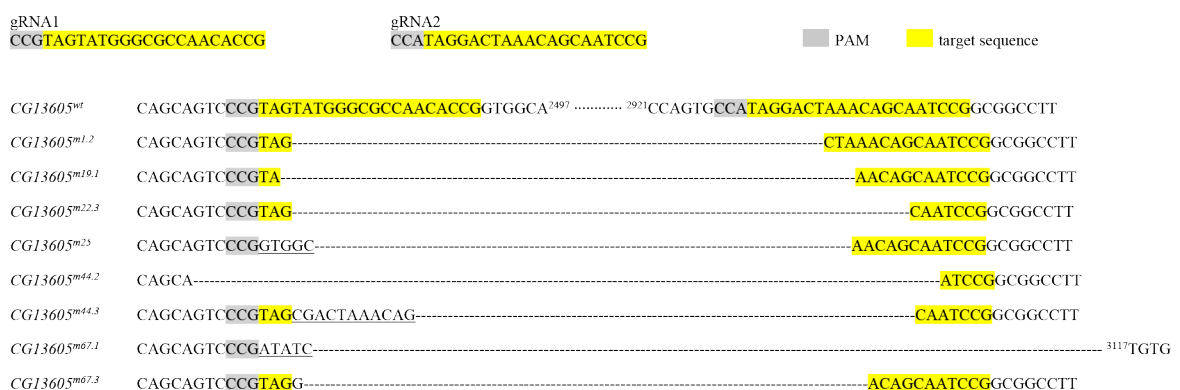


Figure 4.12. Genomic representation of deletion and insertions in the mutant lines. All lines exhibit various number of deletions between gRNAs. *CG13605^{m67.1}* have more deletion than the other lines, *CG13605^{m25}*, *CG13605^{m44.3}*, *CG13605^{m67.1}* and *CG13605^{m67.3}* also have nucleotide insertions at the site of gRNA1.

CG13605 is a 669-amino acid length protein that have a RING finger domain close to the N-terminus of the protein and two putative transmembrane domains. At the protein level, all of the lines are predicted to create much shorter proteins than the wild-type protein (Figure 4.13). Also, two predicted transmembrane domains as well as the RING finger domain were eliminated in each of the mutants except for *CG13605^{m22.3}*. *CG13605^{m22.3}* showed a deletion of 468 bp in the region between the gRNAs. This deletion does not cause any frameshift mutation or early stop codon. Instead, it only creates a 156-aa length deletion. It can also be seen that both predicted transmembrane domains and the RING finger domain are still present in the line *CG13605^{m22.3}*.

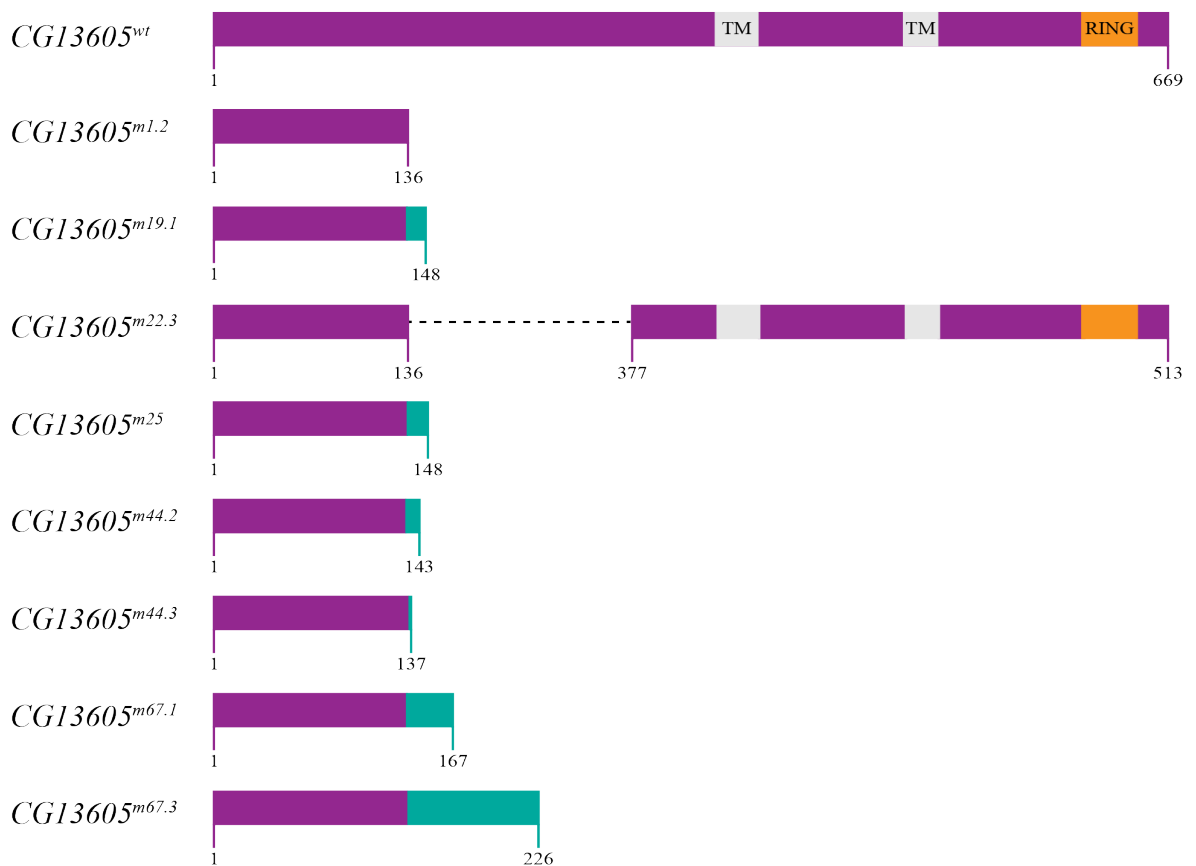


Figure 4.13. Polypeptide representations of the generated mutant lines. Each line has a different length of frameshift mutation, early stop codon and different length of polypeptide chain except for *CG13605^{m22.3}*, it does not have any frameshift mutation or early stop codon.

Since there is not a specific antibody for CG13605, we could not verify the loss of protein.

4.3.3. Morphological Analysis of Mushroom Bodies of *CG13605* Null Mutants

For further functional characterization of *CG13605*, we analyzed the mushroom bodies of eight mutant lines in the adult brain with FasII staining. Four-10 day-old adult flies were used and female and male flies were analyzed separately. To eliminate possible phenotypes that may be resulting from background effects or the presence of balancer chromosomes the eight mutant lines were crossed with a second balancer line (BL24640) whose first and second chromosomes are isogenic with w^{1118} (BL5905). It turned out that all mutant lines are homozygous viable. As can be seen in the Figure 4.14, we have generated eight homozygous viable mutant lines and continued morphological analysis with these lines using w^{1118} as a control.

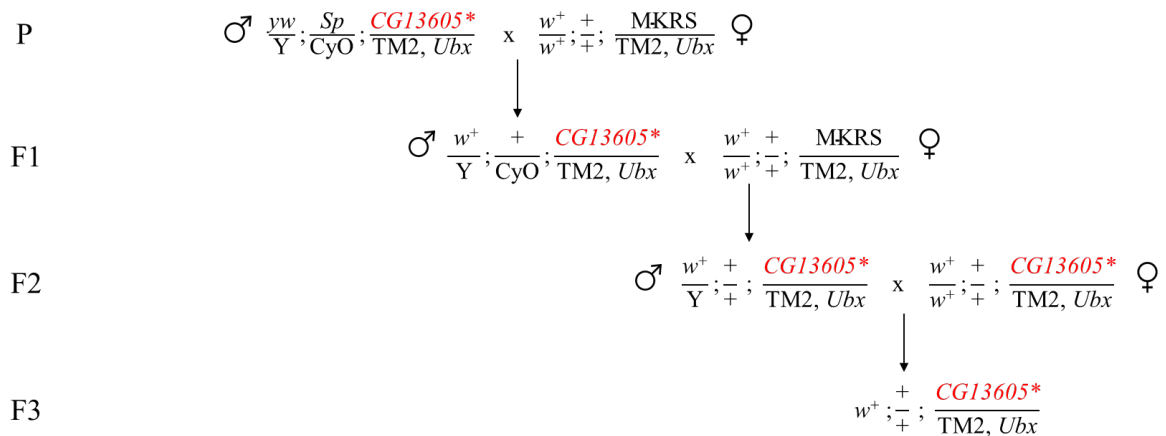


Figure 4.14. Cross scheme of *CG13605* null mutants. In order to eliminate any effects of genetic background or balancer chromosomes, first and second chromosomes of mutant flies were isogenized with w^{1118} flies.

As there are two Kenyon cell clusters on each side of the *Drosophila* brain and they form two separate MBs, MB analyses of mutant lines were conducted as one brain having two mushroom bodies.

Various morphological changes in mushroom body development were observed in different mutant lines. The observed phenotypes include shortening or loss of α/β lobes, misguidance in the α/β lobes, β lobe fusion, thinning/thickening of α/β lobes and branching of α/β lobes. I also observed mild phenotypes such as α lobe shortening and β lobe fusion and more severe phenotypes such as complete loss of α/β lobes or axon branching (Figure 4.15).

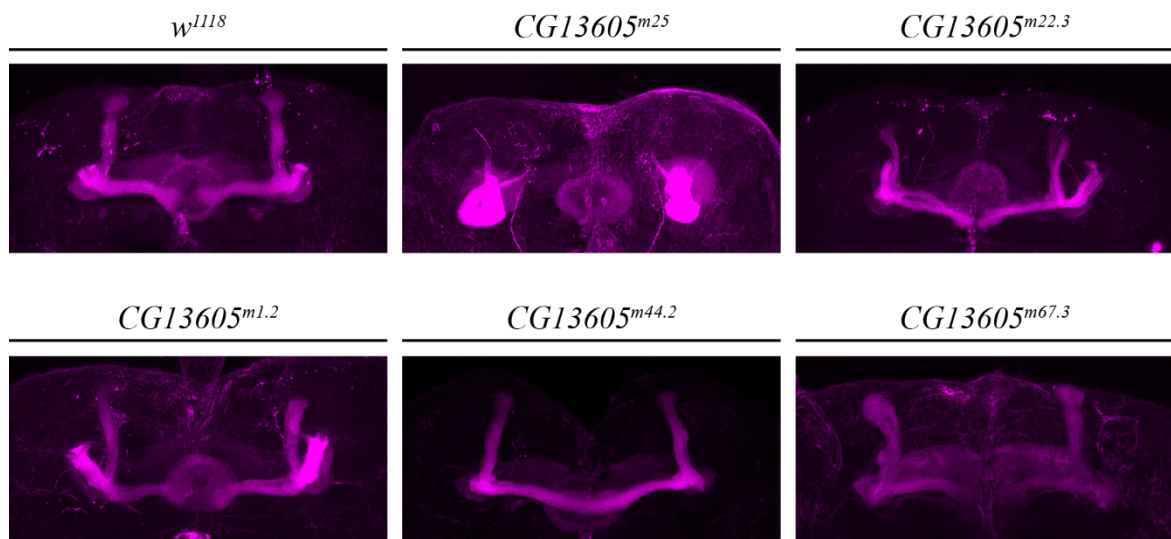


Figure 4.15. Observed phenotypes in the mushroom bodies of the mutant lines. The severity of the phenotypes was various. Mild phenotypes were observed like α shortening, β fusion as well as severe phenotypes like complete loss of α/β lobes or axon branching.

All phenotypes seem to be a kind of misguidance defect.

Interestingly, some brains exhibited more than one phenotype at the same time. For example, in Figure 4.15, the example for the *CG13605^{m22.3}* line shows axon branching and misguidance as well as α shortening. In the example for *CG13605^{m67.3}* both thickening of

α/β lobes and misguidance of α lobe can be observed. In contrast to that, in some brains, there was only one phenotype observed, e.g. α lobe shortening in *CG13605^{m1.2}* β lobe fusion in *CG13605^{m44.2}*. The most severe phenotype I observed was axon stalling, which was present only in the *CG13605^{m25}* line. In these brains, the axons of α/β lobes were not projecting anywhere and were crawling around the cell bodies.

I classified the observed phenotypes into five main categories as axon misguidance (includes α/β shortening, axon branching and misguidance defects), β lobe fusion, axon stalling, α/β lobe thinning/loss and lobe thickening (Figure 4.16.A). In the right part of Figure 4.16, you can see the percentages of each mainly observed phenotypes according to each line and the number of mushroom bodies analyzed for each column as sample sizes (N). There was no significant difference between male and female flies in every line analyzed. The severity and the penetrance of the phenotypes were also not consistent. For example, in the line *CG13605^{m67.1}*, females showed no observable phenotype and only 10% of the males showed mild misguidance phenotype. On the other hand, the lines *CG13605^{m22.3}* and *CG13605^{m25}* showed severe phenotypes and high penetrance in both females and males. 78% of females and 30% of males from *CG13605^{m22.3}* line showed axon misguidance defects. From the line *CG13605^{m25}*, 89% of females and 32% of males showed axon stalling phenotype. Lobe thickening phenotype was present only with the *CG13605^{m67.3}* line, with a frequency of 94% for females and 50% for males.

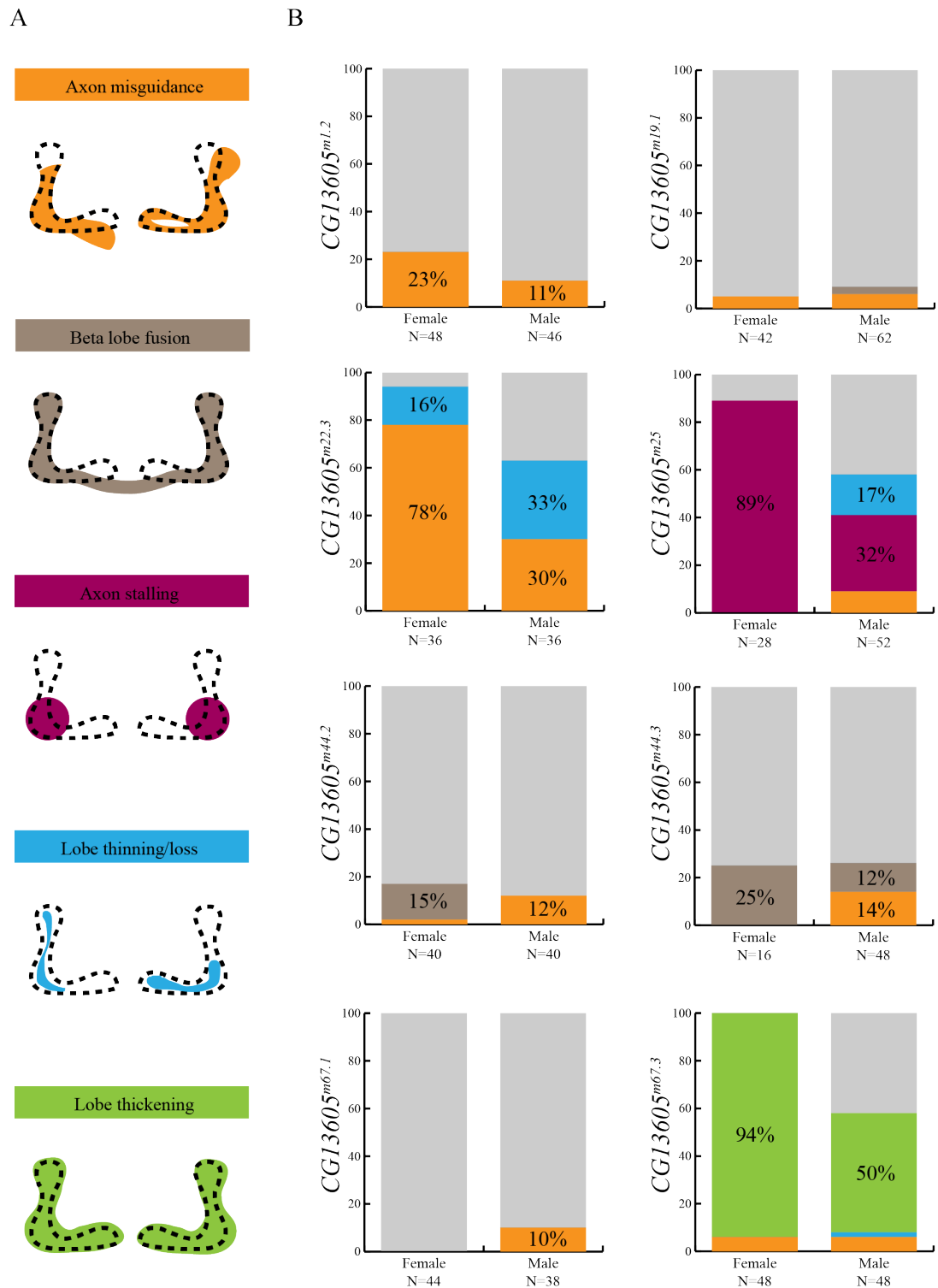


Figure 4.16. Results of morphological analysis of mutant lines. A. Schematic representation of classified phenotypes. B. Percentages of observed phenotypes according to each line and gender. The severity and penetrance of the phenotypes are varying between lines and there are no gender-dependent differences.

Figure 4.17 shows total percentages of observed phenotypes independent of the sex of the flies. The sample size (N) indicates the total number of mushroom bodies that were analyzed for each line. The lines *CG13605^{m22.3}*, *CG13605^{m25}* and *CG13605^{m67.3}* showed the greatest penetrance and one phenotype for each was more dominantly observed. The percentages that are higher than 10% are as indicated in the graph. Axon misguidance, β lobe fusion and lobe thinning/loss phenotypes were also present in the control line but with very low frequencies (2%, 3% and 1%, respectively).

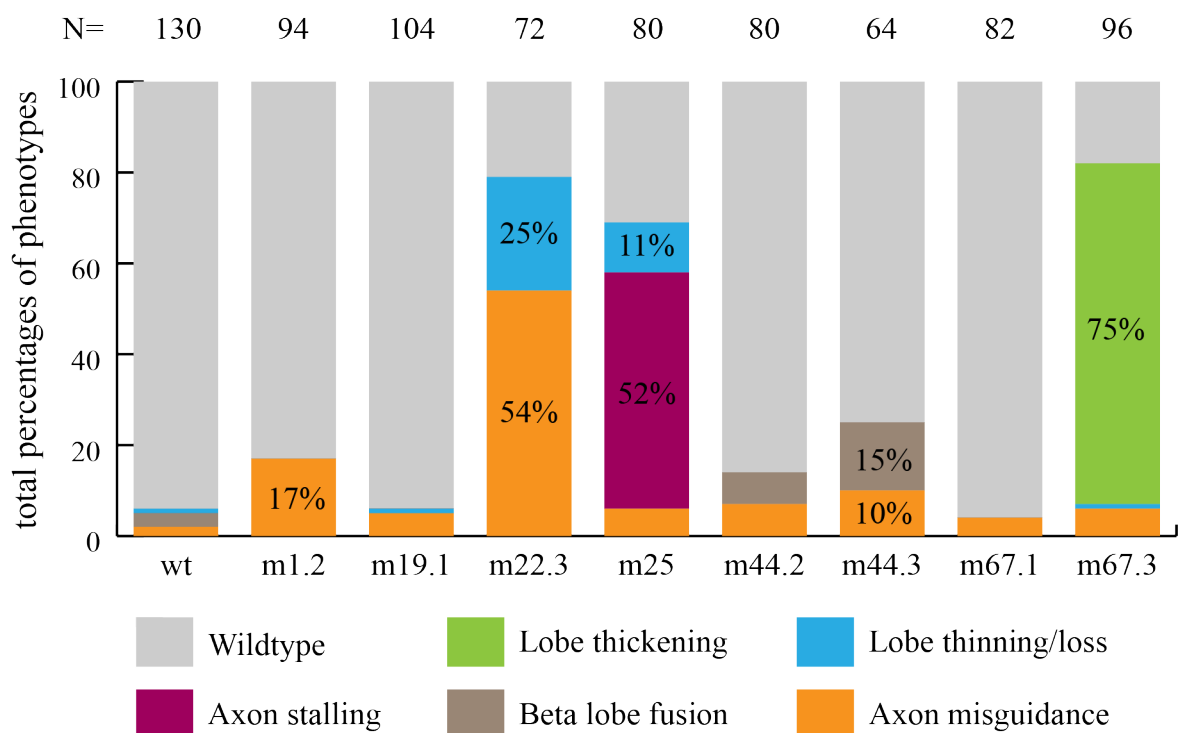


Figure 4.17. Total percentages of observed phenotypes according to each line. Three lines, *CG13605^{m22.3}*, *CG13605^{m25}* and *CG13605^{m67.3}*, have shown more penetrance and more severe phenotypes than remaining five. The most common phenotype is axon misguidance and it is observed in all of the lines. The sample size of each group is indicated on top (N).

In addition to mushroom body phenotypes, homozygous mutant lines also showed a change in the morphology of their brain tissue. Although not in every line, three of the lines (*CG13605^{m22.3}*, *CG13605^{m44.3}* and *CG13605^{m67.1}*) showed a change in their brain tissue composition with varying penetrance (Table 4.5). The brains showed an increase in brain

size pointing to a possible deposition of material at the surface, which could be lipid (Figure 4.18). This accumulation of material at the surface was preventing the light and any fluorescence signal from penetrating and thus less brains could be fully analyzed for MB morphology, especially for the *CG13605^{m44.3}* line where this phenotype was highly penetrant (50% of brains).

Table 4.5. The numbers and percentages of brain phenotypes observed.

	Female	Male	Total
<i>CG13605^{m22.3}</i>	9% (2/21 brains)	15% (3/20 brains)	12%
<i>CG13605^{m44.3}</i>	62% (13/21 brains)	52% (15/29 brains)	56%
<i>CG13605^{m67.1}</i>	4% (1/22 brains)	14% (3/21 brains)	9%

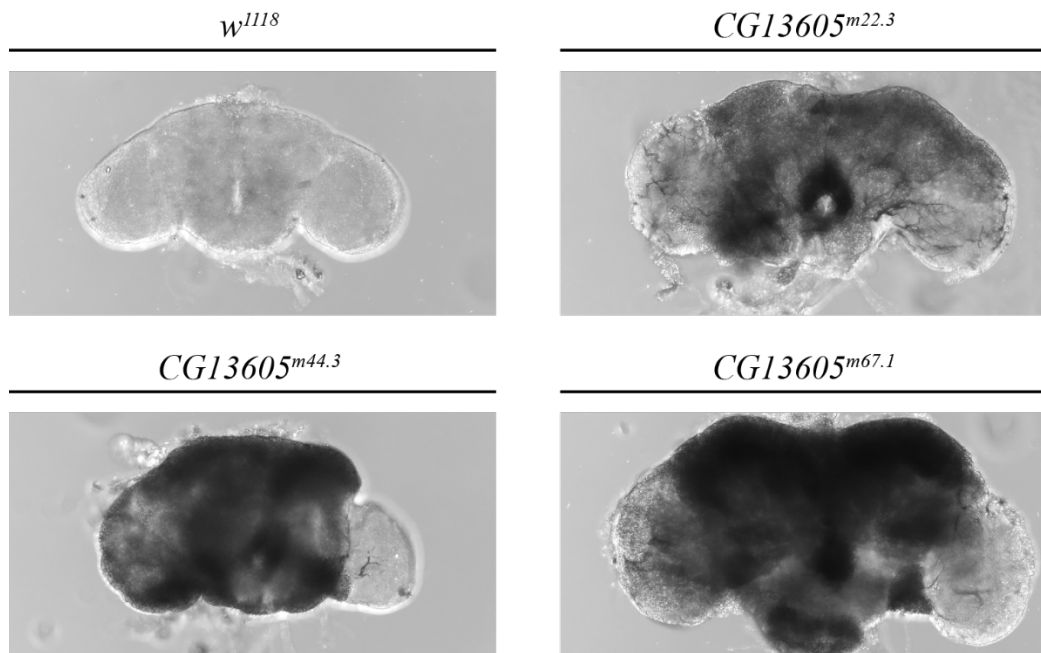


Figure 4.18. Examples of the brain phenotype observed in the mutant lines. The brains were coated with what seems to be lipid and any fluorescence signal was prevented from the brains.

In summary, loss of *CG13605* resulted in both defects in MB development and axon guidance defects and changes in the brain tissue morphology. Even though the severity and the penetrance of the phenotypes are varying, we can suggest that *CG13605* most probably has a role in both MB and brain development. The difference in the penetrance of phenotypes may be resulting from any possible background or epigenetic factors, despite all crosses in order to eliminate those factors.

4.4. Generation and Validation of RNFT2 Expressing Flies

To address the function of RNFT2 and its variant in flies, we generated transgenic lines that express human RNFT2 in its wild type and previously defined variant (c.1150T>C, p.C384R) forms under UAS control. An HA tag was also added to the constructs in order to be able to detect RNFT2 expression in flies since there is not a specific antibody for it.

4.4.1. Generation of RNFT2^{wt} and RNFT2^{C384R} Expressing Fly Lines

The coding sequence of RNFT2 was amplified from HeLa cDNA with the primers RNFT2-F and RNFT2-R which also has attB sequences. The amplified fragment was cloned into the vector pDONR207 via Gateway cloning (Figure 4.19.A) and verified by sequencing. The wild-type fragment was used as a template and by site-directed mutagenesis PCR with the primers SDM_rnft2_fw and SDM_rnft2_rev the c.1150T>C variation was introduced (cloning done with help of Kenneth Schöneck). After verification of the SDM by sequencing, both fragments were cloned into pUASg-HA.attB vector via LR reaction (Figure 4.19.B). pUASg-HA.attB vector is used to express genes under the control of UAS sequences (Bischof *et al.*, 2013). The cloned cDNAs are also tagged with a 3xHA tag at the C-terminus that can be used for verification of the transgenic line and immunostaining. This plasmid also carries an attB site, which enables site-specific integration into fly genome onto an attP-containing docking site via phiC31-mediated integration.

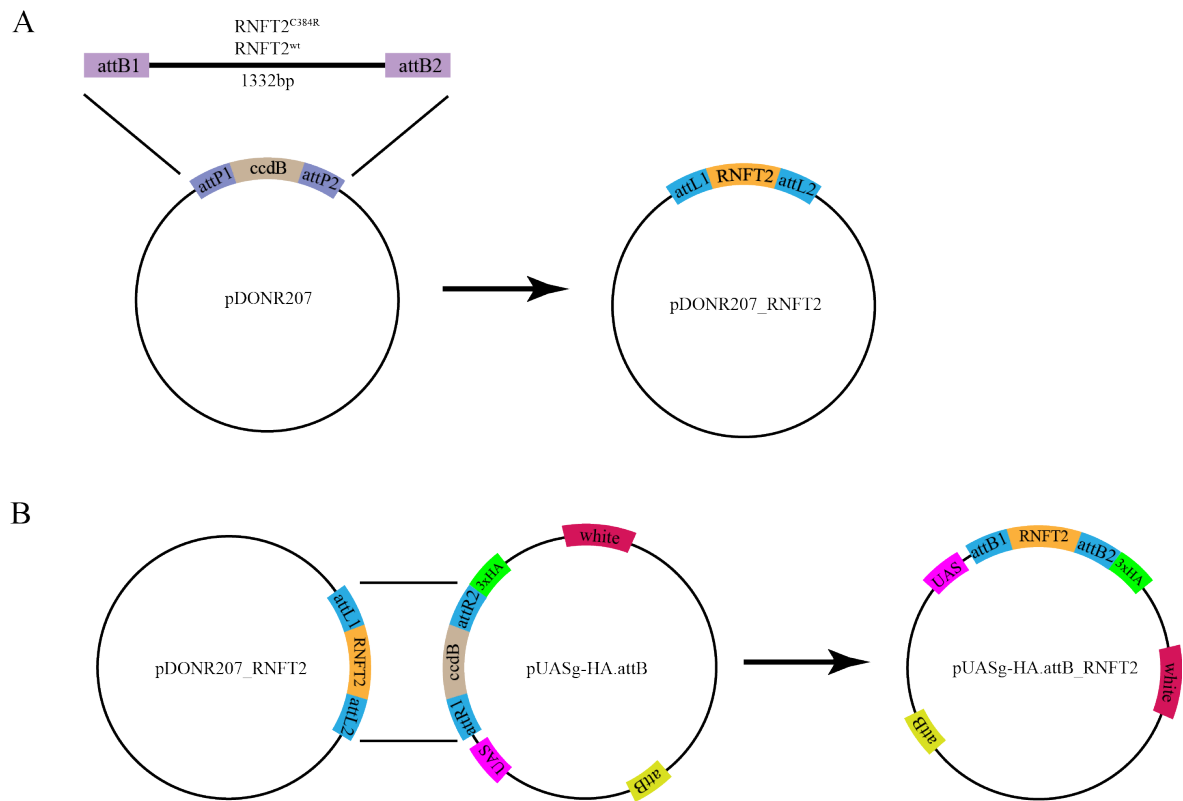


Figure 4.19. Representative schemes of Gateway cloning constructs for RNFT2 expressing lines generation. A. Constructs for BP cloning. Wild type and variant sequences of RNFT2 were amplified with attB site-included primers and cloned into pDONR207 vector. B. Constructs for LR cloning. pDONR207 vectors that include RNFT2 sequences were cloned into pUASg-HA.attB plasmid which carries UAS sequence, 3xHA tag, white gene and attB site for site-specific integration to the genome.

After verification via sequencing, plasmids were injected into 250 fly embryos by the company GenetiVision, USA. The constructs were integrated into the genome on the second chromosome (docking site: aatP40(2L)25C). Positive transformants were selected according to their eye color and generated lines were provided to us by the company. Three transgenic lines were provided to us: *UAS-RNFT2^{wt}*, *UAS-RNFT2^{C384R}* (*m6m1*) and *UAS-RNFT2^{C384R}* (*m1m1*). They were balanced with *ywQB* flies.

4.4.2. *In Vitro* Characterization of RNFT2-Expressing Flies

In order to validate RNFT2 tagging and expression in the generated UAS lines, Western blotting was performed. The three transgenic flies were crossed with *elav^{C155}-Gal4* (BL458) line. Fifteen female and twenty males were homogenized and lysed. Total proteins from whole body was extracted. Protein concentrations were measured and equilibrated with Laemmli sample buffer. Proteins were run on a 7.5% acrylamide gel and then transferred to a PVDF membrane for Western blotting. The membrane was first stained with Ponceau S dye and imaged for visualization of total amount of proteins on the membrane. Then the membrane was blocked and stained with anti-HA antibody in order to detect HA-tagged RNFT2 proteins. Lysate from *elav^{C155}-Gal4* was used as a negative control and lysates from male and female flies were analyzed separately.

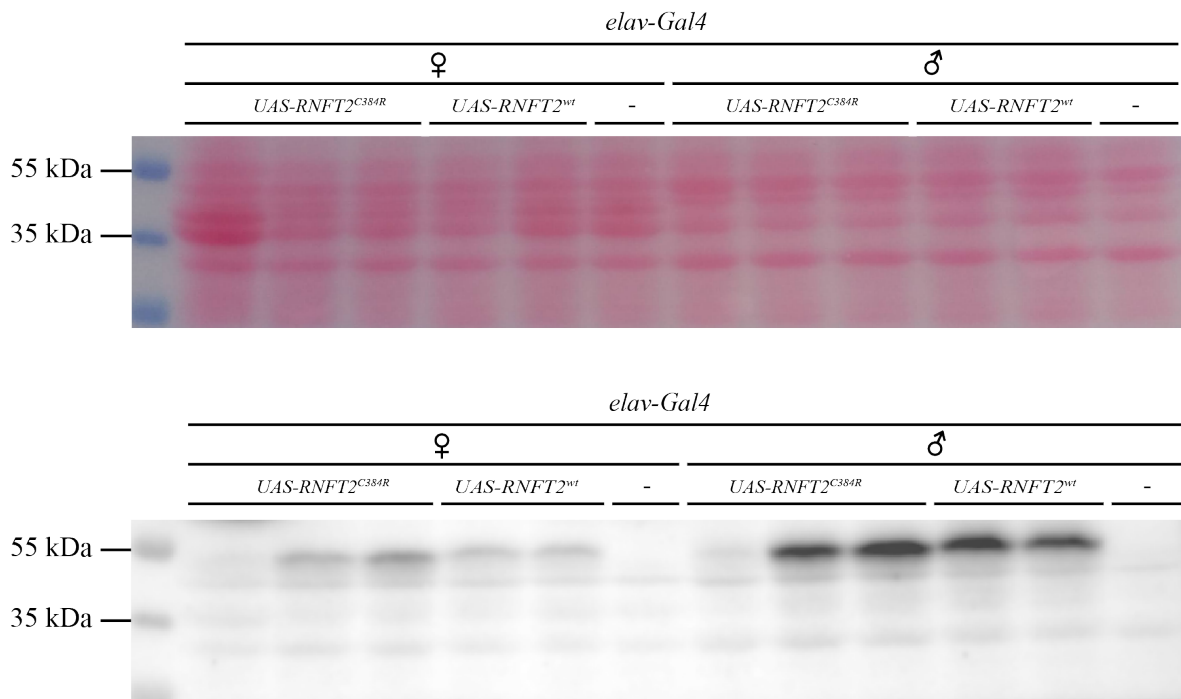


Figure 4.20. Western blot analysis of RNFT2-expressing flies. Membrane was stained with Ponceau S (upper panel) and labeled with anti-HA antibody (lower panel). The bands around ~52 kDa shows that both wild type and mutant RNFT2 are being expressed under Gal4 control.

showed rescued MB phenotypes (Figure 4.22) and bristle phenotypes on their thorax (Figure 4.22).

First, I stained the brains of *CG13605-Gal4>UAS-RNFT2^{wt}; CG13605^{m67.3}* flies, in order to analyze if RNFT2 expression rescues the MB phenotype that was observed in the mutants. The phenotype that I observed with *CG13605^{m67.3}* mutants was α/β lobe thickening with a frequency of 94% for females and 50% for males (Figure 4.16). When RNFT2 is expressed in the mutant background this phenotype was not observed and thus rescued both in males and females (Figure 4.22).

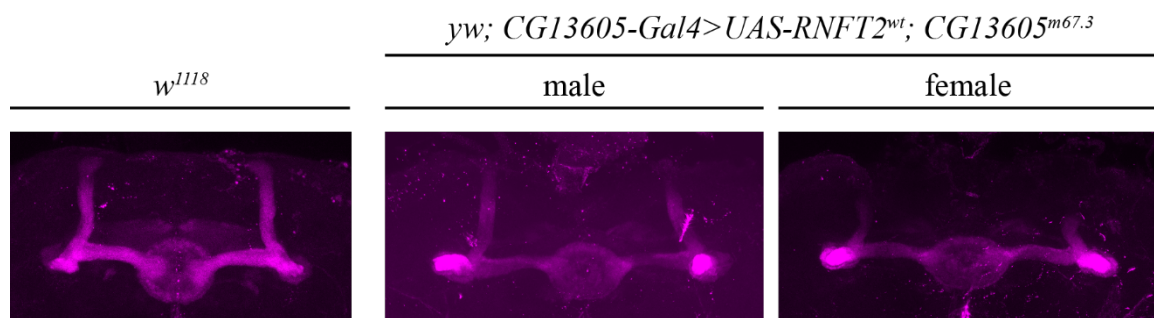


Figure 4.22. Mushroom bodies of rescue flies. Four females and six males were dissected and analyzed. All males showed phenotype rescue on the MBs whereas due to staining problems, the rescue could not be confirmed for α lobes of females.

I was able to dissect only 4 female and 6 male flies and in case of the females a staining problem resulted in images of poor quality that prevented a conclusive analysis of α lobes. However, analysis of β lobes was possible and rescue of the lobe thickening phenotype has been observed. The same observation was made for the male flies where none of the MB lobes showed any thickening phenotype. While further experiments are needed to strengthen this claim my preliminary results indicate that ectopic RNFT2 expression rescues the MB phenotype caused by *CG13605* loss, validating the predicted homology.

Interestingly, the same flies also showed a bristle phenotype on their thorax on both sides (Figure 4.23). Wild type flies have one anterior notoplural and one posterior notoplural bristle on the lateral sides of their thorax (Figure 4.23, arrowheads). However, the rescued flies have more bristles on their lateral thorax, ranging between three to five (Figure 4.23, rectangles). Eight female and six male flies were observed and each of them show more bristles on both their left and right sides. The patterning of bristles on the *Drosophila* thorax is a well-controlled phenotype: *achaete-scute (ac-sc)* genes are expressed in a spatially-restricted manner in cell clusters and mediated by many distinct cis-regulatory elements (Usui *et al.*, 2008). Various genes like Hox genes and signaling pathways like the JNK signaling pathway have a role in bristle patterning (Rozowski and Akam, 2002; Ma *et al.*, 2013). When *CG13605-Gal4>UAS-RNFT2^{wt}* flies were in the wild type background, this phenotype was not observed. Moreover, homozygous mutants were also lacking this phenotype on their bristles.



Figure 4.23. Bristle phenotype on the thorax of rescue flies. Wild type flies have one anterior and one posterior notoplural bristle (arrowheads). The flies that express RNFT2^{wt} under CG13605-Gal4 control in the CG13605^{m67.3} mutant background showed more bristles on their lateral thorax.

It is not entirely clear whether this phenotype only occurs when wild type RNFT2 is expressed in the mutant background because there may be some molecular interactions still going on in both homozygous mutants and RNFT2 expressing flies without resulting in an observable phenotype.

5. DISCUSSION

With the worldwide prevalence of 1-3%, intellectual disabilities continue to be a burden to societies socially and economically. Even though the diagnostic symptoms are well explained and there is an increasing interest to develop treatment strategies for ID, the genetic causes still need to be identified. Thus, next generation sequencing techniques are a great step in the study of revealing ID-related genes.

RNFT2 is found to be an ARID-related gene and in order to enlighten the relationship between *RNFT2* and ID, I utilized *Drosophila melanogaster* as a model organism and tried to unveil the role of *RNFT2* in ID.

5.1. Analysis of the Localization Pattern of CG13605

One critical requirement for a gene to have a role in learning and memory would be its expression in the brain including relevant brain regions. Thus, my first experiment was to characterize the expression pattern of *CG13605*, the fly orthologue of *RNFT2*. As no antibodies for *CG13605* are available I utilized the Gal4/UAS system. Transgenic flies that express Gal4 under the control of the putative promoter region of *CG13605* were generated and crossed to UAS carrying reporter lines. I examined the expression pattern of *CG13605* in the larval, pupal and adult stages.

Staining of *CG13605-Gal4>UAS-nLacZ* larval brains showed that *CG13605* is expressed in neurons rather than glia. This observation was later confirmed with adult brain stainings. Moreover, there was a continuous expression in the Kenyon cells of the MB from larval stages to adulthood. This result suggests that *CG13605* may have a role in the development of the MB. The expression pattern in the adult Kenyon cells with the nLacZ reporter revealed that the *CG13605-Gal4* is expressed in a subset of Kenyon cells. To elucidate whether *CG13605-Gal4* is restricted to one of the Kenyon cell subsets (α/β , α'/β'

or γ Kenyon cells) co-localization studies were attempted, but could not be performed as no subset-specific antibodies are available. The only available tools, subset-specific Gal4 drivers, are not compatible with our own Gal4 line. Thus, I used a combination of *CG13605-Gal4>UAS-mCD8::GFP* and projection-specific antibodies and showed that *CG13605* is expressed in all of the lobes.

In addition to Kenyon cells *CG13605-Gal4* showed expression in other parts of the brain. Cells with prominent expression of *CG13605-Gal4* are located at the dorsal side of the brain whereas another two cells are located ventrally. I did a literature research and found that these dorsally located cells may be Neuropeptide F expressing cells (dNPF). Neuropeptide F signaling and these cells were reported to be mainly important for perception of sensory input, but also for sleep-wake behavior and feeding decisions. On the other hand, the other two cells on the ventral side of the brain were suggested to be descending neurons: carrying signals from brain to the spinal cord. They were found to be involved in sensory-motor coordination and motor control. Unfortunately, I did not have the time and opportunity to further analyze these expressions and cells. However, I propose that *CG13605* may have also an indirect relation to intellectual disability via various pathways including sleep.

While Gal4 lines are an important tool for the study of expression patterns there are a few points that need to be considered when analyzing the results. For example, when the putative promoter region of *CG13605* was cloned, the intergenic region between *CG13605* and *tRNA:Leu-TAA-2-1* was also included in order not to miss any regulatory upstream enhancer. *CG13605* is transcribed from the anti-sense strand and *tRNA:Leu-TAA-2-1* is transcribed from the sense strand. In this case, the intergenic region may also include the regulatory regions of *tRNA:Leu-TAA-2-1*. As regulatory regions can act in both directions, we cannot completely exclude the possibility that the *CG13605-Gal4* line we generated partially reflects the expression of *tRNA:Leu-TAA-2-1*. As no information about the expression pattern of *tRNA:Leu-TAA-2-1* is available the expression patterns of both genes cannot be distinguished from each other at this point. In addition to this possible ‘unspecificity’, I also cannot exclude the possibility of existing trans-regulatory elements of *CG13605*, which lie further away in the genome. As other recent attempts to endogenously

tag genes by CRISPR were unsuccessful we are leaning towards using more classical methods for confirmation of the endogenous expression such as *in situ* hybridization.

5.2. Functional Characterization of CG13605 with Knockdown Experiments

In order to unveil the functions of CG13605, I conducted knockdown experiments using the RNAi system. For this experiment, I utilized a transgenic line expressing shRNA against CG13605 that was generated at the Vienna Drosophila Stock Center: *v105112*. This line belongs to the KK library, which was generated by phiC31-mediated integration of shRNA constructs into the fly genome. The host line of this library *v60100*, which carries the empty vector integrated into the same landing site, but no shRNA construct, was used as control in all knockdown experiments. In addition to antibody staining, I also utilized the *UAS-mCD8::GFP* reporter line to observe morphological changes in the MB.

For MB-specific knockdown of *CG13605*, I utilized three different Gal4 lines. Downregulation by *OK107-Gal4*, which is expressed in all Kenyon cells and *c305-Gal4*, which drives expression in α'/β' Kenyon cells resulted in no observable phenotype, while *c739-Gal4*-driven downregulation resulted in minor alterations in the α/β neurons: thinning in α/β lobes and α lobe misguidance. The thinning phenotype was observed only in females (18%) and α lobe misguidance was present also in control flies with a higher frequency (36% for experimental female flies, 47% for female control flies).

Interestingly, while in one of my preliminary knockdown experiments with *OK107-Gal4* α lobe loss with a frequency of 26% (data not shown) was observed, this phenotype could not be replicated when I repeated this experiment with the same lines. The α lobe loss phenotype is consistent with pan-neuronal knockdown and mutant analysis. This loss of phenotype may be resulting from background effects. There was no observable phenotype also with *c305-Gal4*. I suspect that this indifference may be resulting from the efficiency of *c305-Gal4* line we have. Even though *c305-Gal4* is reported to drive expression only in α'/β' neurons, in our results, a slight expression in α/β neurons can be seen, indicating a possible

leakage in the Gal4 line, resulting in a weakness of driver. Downregulation with *c739-Gal4* resulted in observable phenotypes like α lobe misguidance. This phenotype was however observed in female flies of both experimental and control groups. In males, the same phenotype was not present in the control group while it could be observed in the experimental group. Knockdown of *CG13605* in α/β neurons resulted in a phenotype that is significant in males only. When *CG13605* was downregulated in all MB neurons, α lobe misguidance was not observed, indicating a possible rescue effect coming from the α'/β' and γ neurons. Another phenotype observed with *c739-Gal4* is the thinning of α/β lobes that was observed only in female experimental flies. Whether the axons did not develop in the first place or they were lost during development is still unclear.

After MB-specific knockdown, I utilized two other Gal4 drivers to downregulate *CG13605* expression pan-neuronally. I observed various phenotypes such as α lobe loss or β lobe fusion with varying penetrance in males and females. α lobe loss was present in male flies only when *elav^{C155}-Gal4* was used. On the other hand, β lobe fusion was present in females, with a higher penetrance, when *elav.L2-Gal4* was used. The different phenotypes that were observed with different Gal4 lines may result from the varying efficiency of the Gal4 driver lines as they have been generated in different ways. All observed phenotypes are the result of axonal misguidance. In the MBs α lobe loss and thickening of the β lobe was observed at the same time, indicating that rather than extending towards the dorsal part of the brain, α lobe axons projected following the same pathway as β lobe axons. In the other phenotype, β lobe axons continued to project to the contralateral side of the brain crossing the midline, rather than stalling at the midline.

These results suggest that *CG13605* may play a role in the proper guidance of α/β neuron axons. As an E3 ubiquitin ligase *CG13605* may be modifying proteins that are important for axon guidance during MB development. Another interesting point worth to note is that, when knockdown was performed in MB neurons only, the overall rate of abnormalities was lower than the pan-neuronal knockdown. This difference may indicate a role for *CG13605* in cell-cell interactions. In order to understand the knockdown effects better the knockdown efficiency for both of the experiments should be verified by qRT-PCR.

Furthermore, it would be useful to confirm the results by a second RNAi line (which was however not available), enhancing RNAi effects by adding *UAS-Dicer* to the background or by analyzing a mutant. I proceeded to generate a knock-out mutant for *CG13605*.

5.3. Functional Characterization of CG13605 with Knockout Experiment

For further functional analysis of *CG13605*, I generated *CG13605* null mutants via CRISPR/Cas9. For this aim, two guide RNAs targeting the first exon of *CG13605* were cloned and injected into fly embryos. A transgenic line expressing the gRNAs was generated. Crossing the gRNA carrying transgenic flies with *nos-Cas9* flies made it possible to induce double stranded breaks in *CG13605* to create indel mutations. After all of the crossing and screening steps, I was able to generate eight mutant lines. In each of them different numbers of nucleotides were deleted and/or added between the gRNA target sequences, resulting in various frameshift mutations and early stop codons.

After molecular characterization of the mutants, I analyzed their MB morphologies. Morphological changes were observed for all lines, however the severity and penetrance of phenotypes differed between the lines. The phenotypes ranged from mild ones such as α lobe shortening or β lobe fusion to more severe ones like complete loss of α/β lobes or axon branching. The penetrance of phenotypes was also variable. Some lines such as *CG13605^{m19.1}* or *CG13605^{m67.1}* showed less severe phenotypes as compared to others. Why are various phenotypes observed when all mutations are in the same gene? The answer could be ‘phenotypic heterogeneity’. Phenotypic heterogeneity arises when mutations within a single gene diverge and bring out different phenotypes (Wolf, 1997). These mutations may be affecting different sites of a specific gene but could also be identical (Wolf, 1997). The effects of genetic background are an important factor that can bring about genetic heterogeneity. It was shown that genetic background can alter highly penetrant mutation effects (Kammenga, 2017). While I tried to bring each mutant line to the same background as the control line by back-crossing them, this method does not eliminate genetic background effects completely. Thus, there may be some background effects on the penetrance of the phenotypes. Moreover, epigenetic mechanisms and stochastic effects also were shown to

result in different phenotypes in an isogenic background (Kammenga, 2017). We cannot eliminate these factors easily, so they need to be taken into account during analysis.

In addition to these factors, in the mutants that I generated partially functional polypeptides may be produced in the cell. As there will not be wild-type protein in the cells, partially truncated or shorter polypeptides may result in gain-of-function mutations. Especially for the *CG13605^{m44.3}* line, this possibility became apparent as in this mutant line there is only one amino acid frameshift. When it is compared with *CG13605^{m1.2}*, their amino acid sequences appear to be the same except for one aspartic acid at the end of *CG13605^{m44.3}* polypeptide chain. While these types of shorter peptides tend to be degraded in the cell, their presence or absence should be confirmed. However, as no antibody against *CG13605* is available this experiment could not be performed. Alternatively, one could investigate the effect of the mutation at the mRNA level by performing RT-PCR. This could give an idea about whether the RNA is stable at all and whether a functional protein could be produced.

Crossing each mutant line with each other and analyzing the phenotypic heterogeneity would also be another way to characterize mutations and reduce background effects. The line *CG13605^{m22.3}* is one of the lines that gives rise to increased penetrance and severity both in males and females. According to *in silico* analysis, *CG13605^{m22.3}* shows a deletion of 156-aa without any frameshift or early stop codon. The severity and penetrance of the phenotype may be indicating a functional role for the deleted fragment of the wild type protein.

Structural changes in the MB of the generated mutant lines were my main focus. However, I was only able to investigate possible changes in the adult brains. Analyzing MB structure during early stages of life may give an idea about the role of *CG13605* in MB development. Especially for the *CG13605^{m25}* line, which is found to be losing α/β lobes completely, analyzing larval or pupal MB morphology could be a good approach.

I analyzed MB morphologies using the widely used FasII antibody, which labels α/β lobes. Recently, we were able to obtain a second antibody, namely Trio, which can be used to label α'/β' lobes of the MB (Awasaki *et al.*, 2000). Re-analysis of mutants with this antibody will allow us to determine any α'/β' lobe-specific phenotypes, which might have been missed during analysis with FasII.

In addition to MB phenotypes, some of the lines (*CG13605^{m22.3}*, *CG13605^{m44.3}* and *CG13605^{m67.1}*) displayed a change in brain tissue morphology. The brains were covered with a dense coat of what appears to be lipid and were bigger than wild type brains. As this dense structure on the surface could not be removed by dissection, standard immunostainings of these brains were not conclusive as no fluorescent signals could be recovered due to penetration problems. It is unclear what the cause of this phenotype is. However, there are some possible reasons that may result in such a phenotype. As *CG13605* is a E3 ubiquitin ligase and acts in the protein degradation pathway, it is possible that when mutated, it results in protein aggregation. There are various studies that show when specific proteins are mutated, protein aggregation is observed. For example, when *Drosophila* orthologue of *glucosidase, beta, acid 1* gene, which encodes a lysosomal enzyme, is mutated, proteins that are normally degraded by autophagy were aggregating together and causing behavioral deficits and neurodegeneration (Davis *et al.*, 2016). Autophagy also has been related to protein aggregations in the brain (Jacomin and Nezis, 2018). Moreover, when some human proteins are ectopically expressed in *Drosophila*, protein aggregation was observed (Jeon *et al.*, 2017; Babcock and Ganetzky, 2015). However, all of these examples included protein aggregations in small clusters rather than a broad coating of the brain. Even so, loss of *CG13605* may be affecting ubiquitination and autophagy and more experiments to understand this relation should be conducted. One approach would be investigating the levels of ubiquitination in mutant flies and see how these are changing. Another reason for this phenotype may be related to lipid metabolism. One of our preliminary results showed that the surface tissue could be composed of lipids, rather than proteins (data not shown). It is known that α'/β' and γ Kenyon cells have a role in fat storage regulation (Al-Anzi and Zinn, 2018). Considering all MB phenotypes that I observed, it is possible to claim that the loss of *CG13605* affects fat storage and lipid metabolism in an indirect way.

5.4. Generation and Validation of RNFT2-Expressing Flies and Rescue Experiments

To investigate the orthology between *RNFT2* and *CG13605* and the function of RNFT2 in flies, RNFT2-expressing fly lines were generated. The coding sequences of both *RNFT2^{wt}* and *RNFT2^{C384R}* were cloned into a vector that carries UAS sequence and HA tag and were integrated into the fly genome. Transgenic lines were validated via Western blot analysis. I showed that both wild type and the RNFT2 variant can be expressed when driven by a Gal4. Interestingly, male flies showed a higher level of RNFT2 expression. The reasons for this are not clear at this point.

To analyze the level of orthology between two the fly and human genes, I carried out some crosses to express *RNFT2* under the control of *CG13605-Gal4* in the *CG13605* mutant background. However, due to time limits I was able to conduct crosses for only mutant *CG13605^{m67.3}*. Interestingly, in these flies I observed a bristle phenotype on the lateral thorax. They had more bristles on their lateral (left and right) sides as compared to wild type flies, which have only one anterior notoplural and one posterior notoplural bristle.

Bristle formation on the thorax is a well-characterized phenomenon, which is under the control of various genes and signaling pathways. The main genes that play a role in bristle formation are *achaete* and *scute* (Usui *et al.*, 2008). Furthermore, a gene called *u-shaped* that encodes a zinc finger protein and regulates *achaete* and *scute* during bristle formation, appears to be involved in this process (Cubadda *et al.*, 1997). This gene was also shown to be expressed in the larval fat body (Hyun *et al.*, 2009). In consideration of these findings, ectopically expressed RNFT2 protein may be interacting with proteins that are important in bristle formation. No bristle phenotype was observed in *CG13605-Gal4>UAS-RNFT2* flies in the wild type background. However, even though no macroscopic phenotype was observed, there may be less severe phenotypes and thus these should be analyzed accordingly.

In order to analyze if MB phenotypes that I observed with the homozygous mutants will be rescued with the ectopic expression of wild type RNFT2 I stained adult brains. Homozygous *CG13605^{m67.3}* mutants have shown lobe thickening phenotype in their α/β lobes with high frequency (94% for females, 50% for males). The rescue flies, however, did not display this phenotype, indicating a rescue function of RNFT2 for CG13605 and a preliminary validation of orthology between these two proteins. However, because of some points, this argument is not fully reliable. First of all, the sample sizes of the dissected flies are really low, I could not collect sufficient progeny from the rescue cross due to time limits. In addition, there was a staining problem, most probably because of antibody penetrance, with the female brains and their α lobes were not properly observed. Despite all these problems, β lobes of females and α/β lobes of males displayed wild-type phenotype. In order to consolidate this argument, more experiments need to be conducted. As a first step, the same rescue experiments need to be done for other mutant lines especially for *CG13605^{m22.3}* and *CG13605^{m25}* that showed severe phenotypes. To complete the rescue experiments we are in the process of generating a transgenic line carrying a genomic rescue construct of *CG13605* as well.

As an ultimate experiment to complete the modeling of the RNFT2 ID fly model, the function of the RNFT2 variant in flies needs to be investigated. One would expect that this variant of RNFT2 would not be able to rescue the mutant phenotype and it would be interesting to investigate if and which of the MB phenotypes would be observed. Furthermore, behavioral experiments need to be performed as the link between *CG13605* and learning deficiencies can only be established through behavioral experiments.

In order to further elaborate on the function of the uncharacterized RNFT2 protein we aim to characterize its interaction partners through BioID experiments. For this purpose, we have tagged wild-type and mutant RNFT2 with BirA and are currently awaiting the mass-spectrometry results. Identification of interaction partners would hopefully allow us to confirm that RNFT2 is an E3 ligase. RING finger proteins are not only important for zinc binding but also binding to other proteins such as E2 enzymes (Chasapis and Spyroulias,

2009). We also hope to identify which interactions are lost when the variant is introduced to RNFT2 and thus would lead to unveiling of downstream molecular pathways and functions.

REFERENCES

- Akalal, D. B., C. F. Wilson, L. Zong, N. K. Tanaka, K. Ito, R. L. Davis, 2006, “Roles for *Drosophila* Mushroom Body Neurons in Olfactory Learning and Memory”, *Learning & Memory*, 13, no. 5, pp. 659–668.
- Akalal, D. B., D. Yu, and R. L. Davis, 2010, “A Late-Phase, Long-Term Memory Trace Forms in the γ Neurons of *Drosophila* Mushroom Bodies After Olfactory Classical Conditioning”, *The Journal of Neuroscience: The Official Journal of the Society for Neuroscience*, 30, no. 49, pp. 16699-16708.
- Al-Anzi, B., and K. Zinn, 2018, “Identification and Characterization of Mushroom Body Neurons That Regulate Fat Storage in *Drosophila*”, *Neural Development*, 13, no. 1, pp. 18.
- American Psychiatric Association, 2013, *Diagnostic and Statistical Manual of Mental Disorders*, Fifth Edition, American Psychiatric Publishing, Washington.
- Aradska, J., T. Bulat, F. J. Sialana, R. Birner-Gruenberger, B. Erich, G. Lubec, 2015, “Gel-Free Mass Spectrometry Analysis of *Drosophila Melanogaster* Heads”, *Proteomics*, 15, no. 19, pp. 3356–3360.
- Aso, Y., D. Hattori, Y. Yu, R. M. Johnston, N. A. Iyer, T. T. Ngo, H. Dionne, L. F. Abbott, R. Axel, H. Tanimoto, G. M. Rubin, 2014, “The Neuronal Architecture of the Mushroom Body Provides a Logic for Associative Learning”, *eLife*, 3.

- Aso, Y., K. Grübel, S. Busch, A. B. Friedrich, I. Siwanowicz, H. Tanimoto, 2009, “The Mushroom Body of Adult *Drosophila* Characterized by GAL4 Drivers”, *Journal of Neurogenetics*, 23, no. 1-2, pp. 156–172.
- Awasaki, T., M. Saito, M. Sone, E. Suzuki, R. Sakai, K. Ito, C. Hama, 2000, “The *Drosophila* Trio Plays an Essential Role in Patterning of Axons by Regulating Their Directional Extension”, *Neuron*, 26, no. 1, 119–131.
- Babcock, D. T. and B. Ganetzky, 2015, “Transcellular Spreading of Huntingtin Aggregates in the *Drosophila* Brain”, *Proceedings of the National Academy of Sciences of the United States of America*, 112, no. 39, pp. E5427–E5433.
- Beshel, J. and Y. Zhong, 2013, “Graded Encoding of Food Odor Value in the *Drosophila* Brain”, *The Journal of Neuroscience: The Official Journal of the Society for Neuroscience*, 33, no. 40, pp. 15693–15704.
- Bischof, J., M. Björklund, E. Furger, C. Schertel, J. Taipale, K. Basler, 2013, “A Versatile Platform for Creating a Comprehensive UAS-ORFeome Library in *Drosophila*”, *Development*, 140, no. 11, pp. 2434–2442.
- Bolduc, F. V. and T. Tully, 2009, “Fruit Flies and Intellectual Disability”, *Fly*, 3, no. 1, pp. 91–104.
- Bulayeva, K., K. P. Lesch, O. Bulayev, C. Walsh, S. Glatt, F. Gurganova, J. Omarova, I. Berdichevets, P. M. Thompson, 2015, “Genomic Structural Variants Are Linked With Intellectual Disability”, *Journal of Neural Transmission*, 122, no. 9, pp. 1289–1301.

- Chasapis, C. T. and G. A. Spyroulias, 2009, “RING Finger E(3) Ubiquitin Ligases: Structure and Drug Discovery”, *Current Pharmaceutical Design*, 15, no. 31, pp. 3716–3731.
- Chiu, C. F., Y. Ghanekar, L. Frost, A. Diao, D. Morrison, E. McKenzie, M. Lowe, 2008, “ZFPL1, a Novel Ring Finger Protein Required for Cis-Golgi Integrity and Efficient ER-to-Golgi Transport”, *The EMBO Journal*, 27, no. 7, pp. 934–947.
- Chubak, M. C., K. Nixon, M. H. Stone, N. Raun, S. L. Rice, M. Sarikahya, S. G. Jones, T. A. Lyons, T. E. Jakub, R. Mainland, M. J. Knip, T. N. Edwards and J. M. Kramer, 2019, “Individual Components of the SWI/SNF Chromatin Remodeling Complex Have Distinct Roles in Memory Neurons of the *Drosophila* Mushroom Body”, *Disease Models & Mechanisms*, 12, no. 3.
- Chung, B. Y., J. Ro, S. A. Hutter, K. M. Miller, L. S. Guduguntla, S. Kondo, S. D. Pletcher, 2017, “*Drosophila* Neuropeptide F Signaling Independently Regulates Feeding and Sleep-Wake Behavior”, *Cell Reports*, 19, no. 12, pp. 2441–2450.
- Coll-Tané, M., A. Krebbers, A. Castells-Nobau, C. Zweier, A. Schenck, 2019, “Intellectual Disability and Autism Spectrum Disorders 'On the Fly': Insights from *Drosophila*”, *Disease Models & Mechanisms*, 12, no. 5.
- Cubadda, Y., P. Heitzler, R. P. Ray, M. Bourouis, P. Romain, W. Gelbart, P. Simpson, M. Haenlin, 1997, “*u-shaped* Encodes a Zinc Finger Protein That Regulates the Proneural Genes *achaete* and *scute* During the Formation of Bristles in *Drosophila*”, *Genes & Development*, 11, no. 22, pp. 3083–3095.
- Davis R. L., 1993, “Mushroom Bodies and *Drosophila* Learning”, *Neuron*, 11, no. 1, pp. 1–14.

- Davis, M. Y., K. Trinh, R. E. Thomas, S. Yu, A. A. Germanos, B. N. Whitley, S. P. Sardi, T. J. Montine, L. J. Pallanck, 2016, “Glucocerebrosidase Deficiency in *Drosophila* Results in α -Synuclein-Independent Protein Aggregation and Neurodegeneration”, *PLoS Genetics*, 12, no. 3.
- Dinamarca, M. C., F. Guzzetti, A. Karpova, D. Lim, N. Mitro, S. Musardo, M. Mellone, E. Marcello, J. Stanic, T. Samaddar, A. Burguière, A. Caldarelli, A. A. Genazzani, J. Perroy, L. Fagni, P. L. Canonico, M. R. Kreutz, F. Gardoni, M. Di Luca, 2016, “Ring Finger Protein 10 is a Novel Synaptonuclear Messenger Encoding Activation of NMDA Receptors in Hippocampus”, *eLife*, 5.
- Fagerberg, L., B. M. Hallström, P. Oksvold, C. Kampf, D. Djureinovic, J. Odeberg, M. Habuka, S. Tahmasebpoor, A. Danielsson, K. Edlund, A. Asplund, E. Sjöstedt, E. Lundberg, C. A. Szigartyo, M. Skogs, J. O. Takanen, H. Berling, H. Tegel, J. Mulder, P. Nilsson, J. M. Schwenk, C. Lindskog, F. Danielsson, A. Mardinoglu, A. Sivertsson, K. von Feilitzen, M. Forsberg, M. Zwahlen, I. M. Olsson, S. Navani, M. Huss, J. Nielsen, F. Ponten, M. Uhlén, 2014, “Analysis of the Human Tissue-Specific Expression by Genome-Wide Integration of Transcriptomics and Antibody-Based Proteomics”, *Molecular & Cellular Proteomics: MCP*, 13, no. 2, pp. 397–406.
- Feng, K. L., J. Y. Weng, C. C. Chen, M. B. Abubaker, H. W. Lin, C. C. Charng, C. C. Lo, J. S. de Belle, T. Tully, C. C. Lien, A. S. Chiang, 2021, “Neuropeptide F Inhibits Dopamine Neuron Interference of Long-Term Memory Consolidation in *Drosophila*”, *iScience*, 24, no. 12.
- Foriel, S., P. Willems, J. Smeitink, A. Schenck, J. Beyrath, 2015, “Mitochondrial Diseases: *Drosophila Melanogaster* as a Model to Evaluate Potential Therapeutics”, *The International Journal of Biochemistry & Cell Biology*, 63, pp. 60–65.

- Frints S. G. M., A. Ozanturk, G. Rodríguez Criado, U. Grasshoff, B. de Hoon, M. Field, S. Manouvrier-Hanu, S. E Hickey, M. Kammoun, K. W. Gripp, C. Bauer, C. Schroeder, A. Toutain, T. Mihalic Mosher, B. J. Kelly, P. White, A. Dufke, E. Rentmeester, S. Moon, D. C. Koboldt, K. E. P. van Roozendaal, H. Hu, S. A. Haas, H. H. Ropers, L. Murray, E. Haan, M. Shaw, R. Carroll, K. Friend, J. Liebelt, L. Hobson, M. De Rademaeker, J. Geraedts, J. P. Fryns, J. Vermeesch, M. Raynaud, O. Riess, J. Gribnau, N. Katsanis, K. Devriendt, P. Bauer, J. Gecz, C. Golzio, C. Gontan, V. M. Kalscheuer, 2019, “Pathogenic Variants in E3 Ubiquitin Ligase RLIM/RNF12 Lead to a Syndromic X-linked Intellectual Disability and Behavior Disorder”, *Molecular Psychiatry*, 24, no. 11, pp. 1748–1768.
- Green, E. W., G. Fedele, F. Giorgini, C. P. Kyriacou, 2014, “A Drosophila RNAi Collection is Subject to Dominant Phenotypic Effects”, *Nature Methods*, 11, no. 3, pp. 222–223.
- Guo, Y., T.C. Walther, M. Rao, N. Stuurman, G. Goshima, K. Terayama, J.S. Wong, R.D. Vale, P. Walter, R.V. Farese, 2008, “Functional Genomic Screen Reveals Genes Involved in Lipid-Droplet Formation and Utilization”, *Nature*, 453, pp. 657-661.
- Hakim, Y., S. P. Yaniv, and O. Schuldiner, 2014, “Astrocytes Play a Key Role in Drosophila Mushroom Body Axon Pruning”, *PloS One*, 9, no. 1.
- Heisenberg M., 2003, “Mushroom Body Memoir: From Maps to Models”, *Nature Reviews Neuroscience*, 4, no. 4, pp. 266–275.
- Hsu, C. T. and V. Bhandawat, 2016, “Organization of Descending Neurons in Drosophila Melanogaster”, *Scientific Reports*, 6, no. 20259.

- Hu, H., K. Kahrizi, L. Musante, Z. Fattahi, R. Herwig, M. Hosseini, C. Oppitz, S. S. Abedini, V. Suckow, F. Larti, M. Beheshtian, B. Lipkowitz, T. Akhtarkhavari, S. Mehvari, S. Otto, M. Mohseni, S. Arzhangi, P. Jamali, F. Mojahedi, M. Taghdiri, E. Papari, M. J. S. Banavandi, S. Akbari, S. H. Tonekaboni, H. Dehghani, M. R. Ebrahimpour, I. Bader, B. Davarnia, M. Cohen, H. Khodaei, B. Albrecht, S. Azimi, B. Zirn, M. Bastami, D. Wiczorek, G. Bahrami, K. Keleman, L. N. Vahid, A. Tzschach, J. Gärtner, G. Gillessen-Kaesbach, J. R. Varaghchi, B. Timmermann, F. Pourfatemi, A. Jankhah, W. Chen, P. Nikuei, V. M. Kalscheuer, M. Oladnabi, T. F. Wienker, H. H. Ropers, H. Najmabadi, 2019, “Genetics of Intellectual Disability in Consanguineous Families”, *Molecular Psychiatry*, 24, no. 7, pp. 1027–1039.
- Hyun, S., J. H. Lee, H. Jin, J. Nam, B. Namkoong, G. Lee, J. Chung, V. N. Kim, 2009, “Conserved MicroRNA miR-8/miR-200 and Its Target USH/FOG2 Control Growth by Regulating PI3K”, *Cell*, 139, no. 6, pp. 1096–1108.
- Jacomin, A. C., and I. P. Nezis, 2019, “Assays to Monitor Aggrephagy in Drosophila Brain”, *Methods in Molecular Biology*, 1854, pp. 147–157.
- Jamra R., 2018, “Genetics of Autosomal Recessive Intellectual Disability”, *Medizinische Genetik: Mitteilungsblatt des Berufsverbandes Medizinische Genetik e.V.*, 30, no. 3, pp. 323–327.
- Jeon, Y., S. Lee, M. Shin, J. H. Lee, Y. S. Suh, S. Hwang, H. S. Yun, K. S. Cho, 2017, “Phenotypic Differences Between Drosophila Alzheimer's Disease Models Expressing Human A β 42 in the Developing Eye and Brain”, *Animal Cells and Systems*, 21, no. 3, pp. 160–168.
- Joazeiro, C. A. and A. M. Weissman, 2000, “RING Finger Proteins: Mediators of Ubiquitin Ligase Activity”, *Cell*, 102, no. 5, pp. 549–552.

- Johard, H. A., L. E. Enell, E. Gustafsson, P. Trifilieff, J. A. Veenstra, D. R. Nässel, 2008, “Intrinsic Neurons of *Drosophila* Mushroom Bodies Express Short Neuropeptide F: Relations to Extrinsic Neurons Expressing Different Neurotransmitters”, *The Journal of Comparative Neurology*, 507, no. 4, pp. 1479–1496.
- Jong, M. T., T. A. Gray, Y. Ji, C. C. Glenn, S. Saitoh, D. J. Driscoll, R. D. Nicholls, 1999, “A Novel Imprinted Gene, Encoding a RING Zinc-Finger Protein, and Overlapping Antisense Transcript in the Prader-Willi Syndrome Critical Region”, *Human Molecular Genetics*, 8, no. 5, pp. 783–793, 1999.
- Kammenga J. E., 2017, “The Background Puzzle: How Identical Mutations in the Same Gene Lead to Different Disease Symptoms”, *The FEBS Journal*, 284, no. 20, pp. 3362–3373.
- Kannangara, J. R., M. A. Henstridge, L. M. Parsons, S. Kondo, C. K. Mirth, C. G. Warr, 2020, “A New Role for Neuropeptide F Signaling in Controlling Developmental Timing and Body Size in *Drosophila melanogaster*”, *Genetics*, 216, no. 1, pp. 135–144.
- Kawabe, H., and J. Stegmüller, 2021, “The Role of E3 Ubiquitin Ligases in Synapse Function in the Healthy and Diseased Brain”, *Molecular and Cellular Neurosciences*, 112, no. 103602.
- Keene, A. C., and S. Waddell, 2007, “*Drosophila* Olfactory Memory: Single Genes to Complex Neural Circuits”, *Nature Reviews Neuroscience*, 8, no. 5, pp. 341–354.

- Kim, S., J. Kim, S. Park, J. J. Park, S. Lee, 2021, “Drosophila Graf Regulates Mushroom Body β -Axon Extension and Olfactory Long-Term Memory”, *Molecular Brain*, 14, no. 73.
- Krashes, M. J., S. DasGupta, A. Vreede, B. White, J. D. Armstrong, S. Waddell, 2009, “A Neural Circuit Mechanism Integrating Motivational State with Memory Expression in Drosophila”, *Cell*, 139, no. 2, pp. 416–427.
- Krishna, S. S., I. Majumdar, and N. V. Grishin, 2003, “Structural Classification of Zinc Fingers: Survey and Summary”, *Nucleic Acids Research*, 31, no. 2, pp. 532–550.
- Ma, X., W. Li, H. Yu, Y. Yang, M. Li, L. Xue, T. Xu, 2014, “Bendless Modulates JNK-Mediated Cell Death and Migration in Drosophila”, *Cell Death and Differentiation*, 21, no. 3, pp. 407–415.
- Mabb, A. M. and M. D. Ehlers, 2010, “Ubiquitination in Postsynaptic Function and Plasticity”, *Annual Review of Cell and Developmental Biology*, 26, pp. 179-210.
- Maia, N., M. J. Nabais Sá, M. Melo-Pires, A. P. de Brouwer, Jorge, 2021, “Intellectual Disability Genomics: Current State, Pitfalls and Future Challenges”, *BMC Genomics*, 22, no. 1, pp. 909.
- Mardon, G., N. M. Solomon, and G. M. Rubin, 1994, “*dachshund* Encodes a Nuclear Protein Required for Normal Eye and Leg Development in Drosophila”, *Development*, 120, no. 12, pp. 3473–3486.

- Mariano, V., T. Achsel, C. Bagni, A. K. Kanellopoulos, 2020 “Modelling Learning and Memory in *Drosophila* to Understand Intellectual Disabilities”, *Neuroscience*, 445, pp. 12–30.
- Matthews, J. M. and M. Sunde, 2002, “Zinc Fingers-Folds for Many Occasions”, *IUBMB Life*, 54, no. 6, pp. 351–355.
- Middleton, A. J., J. Zhu, and C. L. Day, 2020, “The RING Domain of RING Finger 12 Efficiently Builds Degradative Ubiquitin Chains”, *Journal of Molecular Biology*, 432, no. 13, pp. 3790–3801.
- Musante, L., and H. H. Ropers, 2014, “Genetics of Recessive Cognitive Disorders”, *Trends in Genetics: TIG*, 30, no. 1, pp. 32–39.
- Nakamura N., 2011, “The Role of the Transmembrane RING Finger Proteins in Cellular and Organelle Function”, *Membranes*, 1, no. 4, pp. 354–393.
- Namiki, S., M. H. Dickinson, A. M. Wong, W. Korff, G. M. Card, 2018, “The Functional Organization of Descending Sensory-Motor Pathways in *Drosophila*”, *eLife*, 7.
- Patel, D. R., M. D. Cabral, A. Ho, J. Merrick, 2020, “A Clinical Primer on Intellectual Disability”, *Translational Pediatrics*, 9, no. Supplementary 1, pp. 23-35.
- Patrick, E., Rajagopal, S., Wong, H., McCabe, C., Xu, J., Tang, A., Imboywa, S., Schneider, J., Pochet, N., Krichevsky, A., Chibnik, L., Bennett, D. and De Jager, P., 2017, “Dissecting the Role of Non-Coding RNAs in the Accumulation of Amyloid and Tau Neuropathologies in Alzheimer’s Disease”, *Molecular Neurodegeneration*, 12, no. 51.

- Pfeiffer, B. D., A. Jenett, A. S. Hammonds, T. T. Ngo, S. Misra, C. Murphy, A. Scully, J. W. Carlson, K. H. Wan, T. R. Lavery, C. Mungall, R. Svirskas, J. T. Kadonaga, C. Q. Doe, M. B. Eisen, S. E. Celniker, G. M. Rubin, 2008, “Tools for Neuroanatomy and Neurogenetics in *Drosophila*”, *Proceedings of the National Academy of Sciences of the United States of America*, 105, no. 28, pp. 9715–9720.
- Port, F., H. M. Chen, T. Lee, S. L. Bullock, 2014, “Optimized CRISPR/Cas Tools for Efficient Germline and Somatic Genome Engineering in *Drosophila*”, *Proceedings of the National Academy of Sciences of the United States of America*, 111, no. 29, pp. 2967–2976.
- Qin, W., C. Liu, M. Sodhi, H. Lu, 2016, “Meta-Analysis of Sex Differences in Gene Expression in Schizophrenia”, *BMC Systems Biology*, 10, no. 9, pp. 99-106.
- Raymond, F. L. and P. Tarpey, 2006, “The Genetics of Mental Retardation”, *Human Molecular Genetics*, 15, no. 2, pp. 110-116.
- Restifo L. L., 2005, “Mental Retardation Genes in *Drosophila*: New Approaches to Understanding and Treating Developmental Brain Disorders”, *Mental Retardation and Developmental Disabilities Research Reviews*, 11, no. 4, pp. 286–294.
- Rezaval, C. (2015). “The Greatness of the Smallest Ones: The Most Valuable Attributes of Flies and Worms for the Study of Neurodegeneration”, In G. N. M. Hagg (Ed.), *Young Perspectives for Old Diseases* (pp. 49-84). Bentham Science Publishers.
- Rozowski, M., and M. Akam, 2002, “Hox Gene Control of Segment-Specific Bristle Patterns in *Drosophila*”, *Genes & Development*, 16, no. 9, pp. 1150–1162.

- Salvador-Carulla, L. and, M. Bertelli, 2008, “‘Mental Retardation’ or ‘Intellectual Disability’: Time for a Conceptual Change”, *Psychopathology*, 41, no. 1, pp. 10-16.
- Sasahara, M., M. Kanda, D. Shimizu, C. Tanaka, Y. Inokawa, N. Hattori, M. Hayashi, G. Nakayama, Y. Kodera, 2021, “Tissue RNFT2 Expression Levels Are Associated With Peritoneal Recurrence and Poor Prognosis in Gastric Cancer”, *Anticancer Research*, 41, No. 2, pp. 609-617.
- Sopko, R., M. Foos, A. Vinayagam, B. Zhai, R. Binari, Y. Hu, S. Randklev, L. A. Perkins, S. P. Perkins, and N. Perrimon, 2014, “Combining Genetic Perturbations and Proteomics to Examine Kinase-Phosphatase Networks in *Drosophila* Embryos”, *Developmental Cell*, 31, no. 1, pp. 114–127.
- Srivastava, A.K. and C. E. Schwartz, 2014, “Intellectual Disability and Autism Spectrum Disorders: Causal Genes and Molecular Mechanisms”, *Neuroscience and Biobehavioral Reviews*, 46 Pt.2, pp. 161-174.
- Tenorio-Castaño, J. A., P. Arias, A. Fernández-Jaén, G. Lay-Son, G. Bueno-Lozano, A. Bayat, L. Faivre, N. Gallego, S. Ramos, K. M. Butler, C. Morel, S. Hadjiyannakis, J. Lespinasse, F. Tran-Mau-Them, F. Santos-Simarro, L. Pinson, A. F. Martínez-Monseny, M. O’Callaghan Cord, S. Álvarez, E. S. Stolerman, C. Washington, F.J. Ramos, The S O G R I Consortium, P. Lapunzina, 2021, “Tenorio Syndrome: Description of 14 Novel Cases and Review of the Clinical and Molecular Features”, *Clinical Genetics*, 100, no. 4, pp. 405–411.
- Tian, Y., Z. C. Zhang and J. Han, 2017, “*Drosophila* Studies on Autism Spectrum Disorders” *Neuroscience Bulletin*, 33, no. 6, pp. 737–746.

- Tong, Y., T. B. Lear, J. Evankovich, Y. Chen, J. D. Londino, M. M. Myerburg, Y. Zhang, I. D. Popescu, J. F. McDyer, B. J. McVerry, K. C. Lockwood, M. J. Jurczak, Y. Liu, B. B. Chen, 2020, “The RNFT2/IL-3R α Axis Regulates IL-3 Signaling and Innate Immunity”, *JCI Insight*, 5, no. 3.
- Tsampoula, M., I. Tarampoulous, T. Manolakou, E. Ninou, P. K. Politis, 2022, “The Neurodevelopmental Disorders Associated Gene Rnf113a Regulates Survival and Differentiation Properties of Neural Stem Cells”, *Stem Cells*, 40, no. 7, pp. 678–690.
- Usui, K., C. Goldstone, J. M. Gibert, P. Simpson, 2008, “Redundant Mechanisms Mediate Bristle Patterning on the Drosophila Thorax”, *Proceedings of the National Academy of Sciences of the United States of America*, 105, no. 51, pp. 20112–20117.
- van der Voet, M., B. Nijhof, M. A. Oortveld, A. Schenck, 2014, “Drosophila Models of Early Onset Cognitive Disorders and Their Clinical Applications”, *Neuroscience and Biobehavioral Reviews*, 46, pp. 326–342.
- Vissers, L. E., C. Gilissen and J. A. Veltman, 2016, “Genetic Studies in Intellectual Disability and Related Disorders”, *Nature Reviews Genetics*, 17, no. 1, pp. 9-18.
- Wieczorek D., 2018, “Autosomal Dominant Intellectual Disability”, *Medizinische Genetik : Mitteilungsblatt des Berufsverbandes Medizinische Genetik e.V*, 30, no. 3, pp. 318–322.
- Wolf U., 1997, “Identical Mutations and Phenotypic Variation”, *Human Genetics*, 100, no. 3-4, pp. 305–321.

Ying, M., X. Huang, H. Zhao, Y. Wu, F. Wan, C. Huang, K. Jie, 2011, “Comprehensively Surveying Structure and Function of RING Domains from *Drosophila Melanogaster*” *PloS One*, 6, no. 9.

Zemirli, N., M. Pourcelot, N. Dogan, A. Vazquez and D. Arnoult, 2014, “The E3 Ubiquitin Ligase RNF121 is a Positive Regulator of NF- κ B Activation”, *Cell Communication and Signaling*, 12, no.72.

Zhao, Y., B. Hongdu, D. Ma, Y. Chen, 2014, “Really Interesting New Gene Finger Protein 121 is a Novel Golgi-Localized Membrane Protein That Regulates Apoptosis” *Acta Biochimica et Biophysica Sinica*, 46, no. 8, pp. 668–674.